A COMPUTATIONAL INSIGHT ON SELF-ETCHING AND BISTYRENIC MONOMERS

by
Gül Beste Özaydın
B.S.,Chemistry, Bogazici University, 2016

Submitted to the Institute for Graduate Studies in
Science and Engineering in partial fulfillment of
the requirements for the degree of
Master and Science

Graduate Program in Chemistry
Boğaziçi University
2019

ACKNOWLEDGEMENTS

First of all, I would like to present my sincere gratitude to my thesis supervisor, Prof. Viktorya Aviyente for welcoming me in her group, allowing me to pursue my studies unrestrainedly and supporting me in every stage of my life. I'm very thankful for her guidance and encouragement. For me, she is not only a mentor but also a role model in many ways that I'm definitely inspired by.

I would like to state my special thanks to Prof. Duygu Avcı for her helpful guidance, to Prof. Dario Pasini for his collaboration and assistance, and to Assoc. Prof. Şaron Çatak for her valuable advices on the research. I would also express my gratitude to Assoc. Prof. Oktay Demircan, Prof. Rana Sanyal, Prof. Tereza Varnalı, and Assoc. Prof. Ece Bulak for their invaluable support throughout my educational life at Bogazici University. The doors to their office were always open whenever I had a question.

I want to place on record, giving thanks to Prof. Stephen Hashmi for allowing me to train in his lab in Heidelberg University, where I found the driving force to continue my studies after completing my bachelor's degree. I would like to express my special thanks to Prof. Maria João Ramos and Prof. Pedro Fernandes for their support to improve myself in the field of computational biochemistry. I would like to thank Rui Neves, Diana Gesto and Paula Juric for their contributions to my learning process during the training in the University of Porto.

I would like to express my thanks to Oğuzhan Kucur, Semiha Kevser Bali, Öyküm Avcı, Taylan Turan, Esma Boydaş and every member in this group (either here or gone), for all the support, patience and company that they have offered me. I would like to state my appreciation to Canan Güler, Melek Naz Güven, Yiğitcan Eken, and Furkan Işık for their invaluable support, help, and friendship.

I'm also thankful to my friends Cansel Baturay, Pınar Alp, Serap Başkır, Selen Gökçe, Yağmur Avcı, and Dença Marancı for being a part of my most important moments, cheering me up and giving me strength in every phase of my life. They are one of the biggest sources of my motivation and the reasons for which I feel lucky.

Last but not least, my deepest gratitude goes to all my family for their endless love and support throughout my life, this dissertation would be simply impossible without them. I will be endlessly thankful for the care and love of my aunts, Nazan Göktaş, Nalan Yangil, and Birsen Odyakmaz. I am thankful to my father Kamil Özaydın, to my grandparents Erol Yangil, and Behice Yangil, who are the people that have been role models to me, for making me believe that any achievement is possible if I work and desire enough. I also owe my thanks to Ümit Elmasoğlu for his constant motivation and support. I am forever grateful to my mother, Handan Özaydın, for initiating the curiosity in me when I was a little kid, for making everything easier, and for giving me the opportunities that have made me who I am. I'm very glad and blessed to have a mother like her. She has been the reason for my smile and has been the light of my way.

This journey would not have been possible without these great people and I dedicate this milestone to them, especially to my mother, who believed in my potential without any doubt, and repeated over and over again that I was capable of great achievements.

ABSTRACT

A COMPUTATIONAL INSIGHT ON SELF-ETCHING AND BISTYRENIC MONOMERS

Cyclopolymerization reaction of difunctional styrene monomers and the efficient binding of self-etching monomers to the hydroxyapatite component of the tooth have been widely studied using empirical approaches. However, the literature lacks a relevant computational basis to supplement such findings. Therefore, this thesis aims at bringing a computational insight into the i) cyclopolymerization reaction of difunctional styrenic monomers and ii) self-etching monomers in dental applications.

In the first part of this work, the synthesis and the efficient cyclopolymerization of difunctional monomers containing styrene moieties tethered each other by the dichlorodiphenylsilane, the dichloro(methyl)phenylsilane and malonate ester protecting groups are illustrated. The experimental findings are rationalized theoretically by tackling the initial steps of cyclopolymerization reaction such as initiation, cyclization, propagation.

In the second part, self-etching monomers and pre-nucleation complexes are modeled by computational protocols. These monomers are of interest in the dental adhesive system applications due to their strong binding to the hydroxyapatite component of the tooth. In order to analyze the strength of the interaction between calcium (HAP) and acid groups (self-etching monomer), pre-nucleation complexes (PNC), have been considered. The interaction between monomers and pre-nucleation complex is examined by the calculation of dissociation energy and the evaluation of NPA charges for PNC-monomer complexes. The computational findings have supported the experimental stability order of the monomers, The computational approach enables the scope of the evaluation of newly designed monomers to be wide in a short period of time without high experimental cost.

ÖZET

KENDİNDEN ASİTLİ VE STİRENİK BİFONKSİYONEL MONOMERLERE HESAPSAL YAKLAŞIM

Çift fonksiyonlu stiren monomerlerinin siklopolimerizasyon reaksiyonu ve kendinden asitli monomerlerin dişin hidroksiapatit bileşenine etkin şekilde bağlanması deneysel yaklaşımlar kullanılarak geniş ölçüde incelenmiştir. Ancak, literatürde bu bulguları desteklemek için uygun bir hesapsal çalışma yapılmamıştır. Bu nedenle, bu tezde, i) çift fonksiyonlu stirenik monomerlerin siklopolimerizasyon reaksiyonunun ve ii) dental uygulamalarda kendinden asitli monomerlerin; hesapsal yöntemlerle incelenmesi amaçlanmaktadır.

Bu çalışmanın ilk bölümünde, diklorodifenilsilan, dikloro(metil)fenilsilan ve malonat ester koruma grupları tarafından birbirine bağlanmış stiren grupları içeren iki fonksiyonlu monomerlerin sentezi ve verimli siklopolimerizasyonu gösterilmektedir. Deneysel bulgular, başlatılma, siklizasyon, ilerleme gibi siklopolimerizasyon reaksiyonunun ilk adımlarının ele alınmasıyla teorik olarak rasyonelleştirilmiştir.

İkinci bölümde, kendinden asitli monomerler ve ön-çekirdeklenme kompleksleri, hesaplama protokolleri ile modellenmiştir. Bu monomerler, dişin hidroksiapatit bileşenine güçlü bağlanmalarından dolayı diş yapıştırma uygulamalarında ilgi çekmektedir. Kalsiyum (HAP) ve asit grupları (kendinden asitli monomer) arasındaki etkileşimin gücünü analiz etmek için çökeltme sırasında hidroksiapatit oluşumuna yol açan ön çekirdeklenme kompleksleri (PNC) dikkate alınır. PNC ile monomer etkileşimini incelemek için her monomerin ayrışma enerjisi hesaplanmıştır. NPA yükleri PNC-monomer komplekslerinin elektronik özelliklerini anlamak için değerlendirilmiştir. Sonuç olarak, hesaplamalı bulgular deneysel çalışmalardan elde edilmiş monomerlerin bağlanma kuvveti ile ilgili bulguları desteklemiştir. Hesaplamalı yaklaşım, yeni tasarlanmış monomerlerin değerlendirmesinin kapsamının yüksek deneysel maliyet olmadan kısa sürede geniş çerçevede yapılabilirliğini ortaya koymuştur.

TABLE OF CONTENTS

LIST OF FIGURES

LIST OF TABLES

LIST OF SYMBOLS

E_b	Binding energy
E_d	Dissociation energy
E_{el}	Electronic and zero-point energy
$E_c[\rho]$	Correlation energy
$E_{KE}[\rho]$	Kinetic energy
$E_x[\rho]$	Exchange energy
$E_{xc}[\rho]$	Exchange and correlation energy
$J[\rho]$	Coulomb energy
$T_s[\rho]$	Kinetic energy of non-interacting electrons
U_x^{σ}	Exchange energy density
$V_{\text{ext}}(\mathbf{r})$	External potential
V_{KS}	Kohn-Sham potential
ΔE_b	Relative binding energy
ΔE_d	Relative dissociation energy
ΔE_{el}	Relative electronic and zero-point energy
ΔE_{rxn}	Heat of reaction as electronic energy
ε_i	Kohn-Sham orbital energy
v(r)	External potential
ρ(r)	Electron density
ψi	Kohn-Sham orbitals
Ψ	Many electron wavefunction

LIST OF ACRONYMS/ABBREVIATIONS

AAS	Atomic Absorption Spectroscopy
ACP	Amorphous Calcium Phosphate
B3LYP	Becke-3-parameter Lee-Yang-Parr functional
CID	Collision-induced Dissociation
DFT	Density Functional Theory
FT-IR	Fourier Transform Infrared Spectroscopy
GGA	Generalized Gradient Approximation
$\hat{H}$	Hamiltonian operator
h_i	One-electron hamiltonian
HAP	Hydroxyapatite
HF	Hartree-Fock
KS	Kohn-Sham
LDA	Local Density Approximation
M06-2X	Empirical exchange-correlation functional
NMR	Nuclear Magnetic Resonance spectroscopy
NPA	Natural Population Analysis
PNC	Pre-nucleation Complex
PM3	Parameterized Model number 3
SEM	Scanning Electron Microscopy
μTBS	Microtensile Bond Strength

1. INTRODUCTION

The rapid growth in the industrialization brought along man-made polymers into every stage of life. At the broadest level, polymers are subdivided into two categories: the synthetic polymers and the natural polymers. Both are obtained through the chemical reaction of monomers, which form the structural units of the polymer chains. Through the production of various types of monomers, new materials are produced and used in many fields from medication to nutrition and to transportation, clothing and adhesive systems [1, 2]. Among all monomers, styrene and acrylic monomers have been the focus of attention due to their wide range of functionality and ability to provide different materials with different physical properties .

Styrene is an organic compound having the formula $C_6H_5CH=CH_2$ which is also known as ethenly benzene, vinylbenzene, and phenylethylene. In order to polymerize styrene to polystyrene, the radical polymerization method is widely used given the presence of double bonds on the vinyl group. In the polymerization, the carbon-carbon π bond of the vinyl group is broken by the radical attack and a new carbon–carbon σ bond is formed, allowing the new radical to react with another monomer [3]. The stereochemistry of the chiral carbon on the styrene determines the tacticity. This has a crucial impact on the physical properties of polystyrene. As an example, the random array of benzene groups forms atactic polystyrene having a lower glass transition temperature compared to the isotactic polystyrene, which is commercially not available [4].

To obtain the desired physical properties of polystyrene, the control over the sequence of monomeric units and their connections within the macromolecular chains has become one of the mainstays of the polymer research. Although such control naturally manifests itself in biological systems, such as enzymes or cytochromes, it is very difficult to achieve it efficiently in artificial settings [5]. In that regard, cyclopolymerization reactions have attracted great interest in the past, coupled with the design of innovative macromolecular architecture [6].

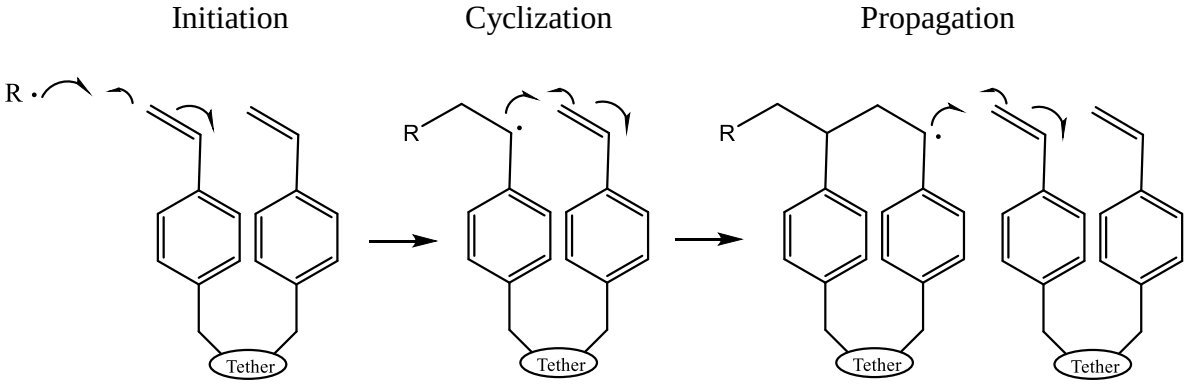

Figure 1.1. Free radical cyclopolymerization of bistyrenenic monomers.

The alternating intra-intermolecular chain mechanism of cyclopolymerization has the ability to warrant alternation, and thus sequence control [7]. This is possible when the monomer is suitably designed with two functionalities with very different reactivities toward the propagating chain. The reactivity of styrene-based systems is hampered by the large ring-forming cyclizations, inevitably competing with crosslinking pathways. As such, interest in the realization of styrenic difunctional monomers undergoing efficient cyclopolymerization has aroused great interest recently. Usually, the two polymerizable aromatic molecules are linked through a “tether” linking group, which is a sterically demanding moiety and works as a directing system favoring cyclization.

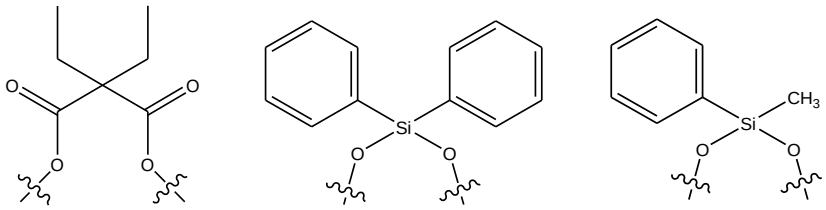

Figure 1.2. Malonate ester, diphenyl silyl and (methyl)phenyl silyl-based tethering groups, respectively.

Previously, the efficient cyclopolymerization of bistyrenic monomers with malonate ester tethering group has been shown by Dario Pasini *et al*. [8]. Then, silyl based monomers have also been proposed as alternative structures to malonate esters due to their advantages over malonate ester groups, such as being commercially available and easy to deprotection.

In this dissertation, the experimental findings of Dario Pasini *et al.* are rationalized by the computational approach to the efficient cyclopolymerization of two new difunctional monomers containing styrene moieties tethered to each other by diphenyl silyl and (methyl) phenyl silyl-based protecting groups (Fig.1.2). To that end, silyl-based tethering groups are selected for this work. Computational methods are applied to compare bistyrenic monomers having malonate ester and silyl-based tethering groups.

On the other hand, methacrylic monomers have been commonly used in dental adhesive systems, where the main goal is to repair various tooth damages such as cracks or gaps. The desired material is obtained through the free radical polymerization of the methacrylic part of the monomers. In addition to the efficient polymerization of the monomers, stable and durable interaction between the polymeric matrix and hydroxyapatite content of enamel is provided by the acidic part of the monomers [9]. Thus, the strength of interaction is the principal interest to increase the efficiency of adhesives. In the last generation of adhesive systems, self-etching monomers, which have phosphonic or phosphoric groups in one end and a polymerizable methacrylic group on the other end, has been proposed (Fig. 1.3) [10].

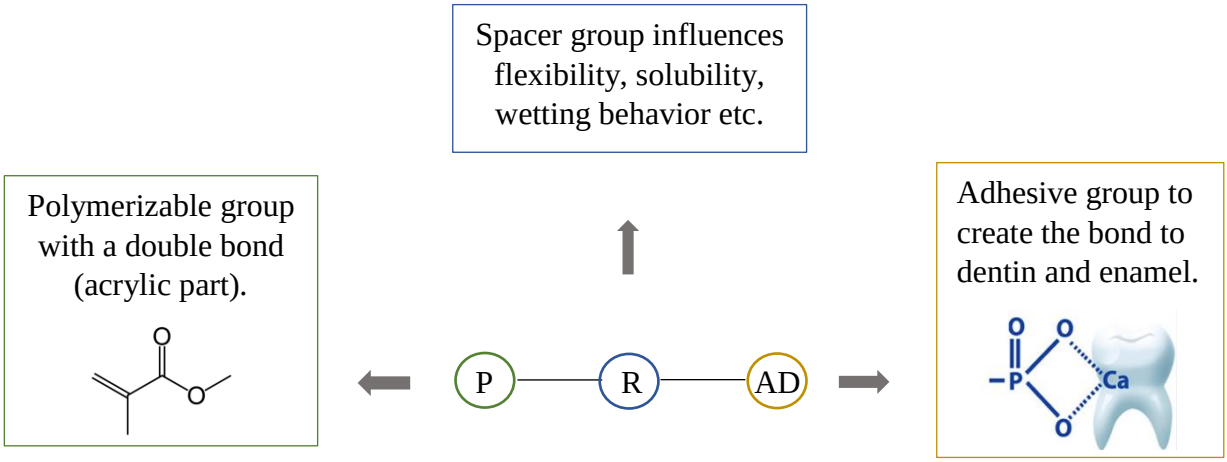

Figure 1.3. Components of self-etching monomers.

The common features of these monomers are the presence of a polarizable group (P) that reacts with the other cross-linking or monofunctional monomers, and an acidic part (AD) which can etch the dental surface to interact with the hydroxyapatite component of

dentin. They also contain a spacer group R to control solubility, elasticity and wetting properties of the monomer [10].

The interaction between the calcium ion located on the hydroxyapatite surface of enamel and the acidic end of the monomer (phosphonic and phosphoric) plays a crucial role in the usage of the adhesive materials. Several studies have been carried out in the last decades, allowing the comparison of the binding efficiency of self-etching phosphoric [11] and phosphonic acid monomers [12]. Phosphoric acid monomers such as MEP, MTEP, CAP-P, MDP, MDDP have different spacer groups (R), whereas the phosphonic acid monomers such as MAEPA, EAEPA, HAEPA have the same spacer group, but differs in acrylic polymerizable components they contain.

In this dissertation, self-etching monomer interaction with the hydroxyapatite component of dentin is tackled by using pre-nucleation complexes as representative structures for hydroxyapatite component of the tooth [13]. The proper conformation of pre-nucleation complex, $[Ca(HPO_4)_3]^{4-}$, is proposed and the chemical interaction analysis is performed by the computational tools.

2. OBJECTIVE AND SCOPE

The control of free radical polymerization technique has been improved by cyclopolymerization reaction of styrene monomers [14]. Passini *et al.* have carried out several studies with different bistyrenic monomers [8]. In this dissertation, a computational approach has been brought to the cyclopolymerization reaction of bistyrenic monomers.

The driving motivation of the first chapter of this thesis is to investigate the initial steps of cyclopolymerization reaction of bistyrenic monomers with different tethering groups. Specifically, we aim at illustrating the energy barriers of the initial steps of the free radical cyclopolymerization reaction. Depending on the energetic differences in each step of the reaction, the efficiency of tethering groups was compared.

The second chapter of this thesis concerns dental adhesive systems, which are widely used to repair dentin surface by forming chemical bonds with the hydroxyapatite component of enamel. Since self-etching monomers have started to be used, several experimental studies have been carried out to improve the bonding and to obtain better properties of the monomers. However, aside from a very few computational studies [15], there has been no generalizable procedure to assess the electronic properties and the bonding between hydroxyapatite and self-etching monomers. Therefore, we aim to evaluate these interactions by using Density Functional Theory to bring a computational perspective at an atomic level. For this purpose, pre-nucleation complexes are taken into account in order to represent hydroxyapatite component of enamel and to provide fast evaluation methodology for self-etching monomer interactions.

Although it is known that pre-nucleation complexes are the spherical calcium triphosphates which form hydroxyapatite surface through precipitation, a consensus has not been reached on their conformational structure and the exact formula. Therefore, as an initial step, a structure search for the pre-nucleation complex is performed and then, self-etching monomer interactions with the selected pre-nucleation complex is carried out.

3. THEORETHICAL BACKGROUND

3.1. Density Functional Theory

Density Functional Theory (DFT), is a quantum mechanical approach to the electronic structure of atoms and molecules [16]. The theory provides an approximate solution to Schrödinger equation of many electron systems [17]. It is based on the calculations of the total electronic energy and the overall electronic density distribution. Hohenberg and Kohn (in 1964) have proposed that the electron density can be used to find the ground-state energy and some other properties of systems. Therefore, the energy is expressed by the functional of electron density ρ(r), which is also a function of space and time. The privilege of the use of electron density as a functional, is the reduced number of variables which is only three spatial coordinates (x,y,z), whereas the variables for the wavefunction of many electron systems are 3N, the coordinates of all N number of atoms in the system.

The electron density is defined as [16];

$$\rho(\mathrm{r})=\mathrm{N}\int\cdots\int|\Psi(\mathrm{r}_1,\mathrm{r}_2,\cdots,\mathrm{r}_{next})|^2\mathrm{dr}_1\mathrm{dr}_2\cdots\mathrm{dr}_n \tag{3.1}$$

where *r* represents both spin and spatial coordinates of electrons. In DFT, the energy is expressed by the two terms as a function of electron density;

$$E[\rho(\mathrm{r})]=\int \mathrm{V}_{ext}(\mathrm{r})\,\rho(\mathrm{r})\mathrm{dr}+\mathrm{F}[\rho(\mathrm{r})] \tag{3.2}$$

where $V_{ext}(r)\,\rho(r)dr$ is used to describe the interaction of electrons with an external potential $V_{ext}(r)$, which is mostly the coulomb interaction with the nuclei. On the other hand, the sum of the kinetic energy of electrons and the contribution from interelectronic interaction is defined by the term $F[\rho(r)]$ [16].

In 1965, one of the biggest contributions to density functional theory is made by Kohn and Sham. A new approach was introduced to the problem with equation 3.2 which was undefined $F[\rho(r)]$. The equation is improved by tackling $F[\rho(r)]$ function as a sum of three terms;

$$F[\rho(r)]=E_{KE}[\rho(r)]+J[\rho(r)]+ E_{XC}[\rho(r)] \tag{3.3}$$

where $E_{KE}[\rho(r)]$ is the kinetic energy of the non-interacting electrons, $J[\rho(r)]$ is the electron-electron coulombic energy which is also known as Hartree electrostatic energy. $J[\rho(r)]$ is the sum of pairwise electrostatic energy between two charge densities and $E_{XC}[\rho(r)]$ is the exchange-correlation energy including the contribution of exchange and correlation, also the kinetic energy difference between interacting (true kinetix energy of the system) and non-interacting electrons ($E_{KE}[\rho(r)]$). Therefore $E_{XC}[\rho(r)]$ is expressed as the sum of exchance $E_X[\rho(r)]$ and correlation $E_C[\rho(r)]$ functionals.

In Kohn Sham density functional theory, Kohn-Sham equation is defined as the one electron Schrödinger equation of a reference non-interacting particle system which generates the same density as any given system of interacting particles. The lowest energy solution to Kohn-Sham equations is provided by the Kohn-Sham wavefunction which is a single Slater determinant genereted by a set of independent orbitals, Ψ_i.

$$\left[-\frac{1}{2}\nabla^2+V_{KS}\right]\Psi_i=\varepsilon_i\Psi_i \tag{3.4}$$

Here, ε_i is defined as the Kohn-Sham orbital energy. The Kohn –Sham equation (3.4) is defined by local external Kohn Sham potential, V_{KS}, in which the non-interacting particles move.

$$V_{KS}= v(r)+\frac{\partial J[\rho]}{\partial\rho(r)}+\frac{\partial E_{XC}[\rho]}{\partial\rho(r)} \tag{3.5}$$

$$V_{KS} = v(r) + \frac{\rho(r')}{|r-r'|} dr' + v_{XC}(r) \quad (3.6)$$

Here, $v_{XC}(r)$ is the exchange-correlation potential. The density for an N-particle system is;

$$\rho(r) = \sum_i^N |\Psi_i|^2 \quad (3.7)$$

if the exact form of the exchange-correlation functional is known. However, the exact form of this functional is not known,therefore, exchange-correlation functionals are developed.

3.2. General Approach to Exchange-Correlation Density Functionals

The challange of the exchange-correlation effect in the assumption is the integration of the fact that electrons are interacting particles. Since the wave function of electron depends on the position and spin momentum of other electrons in the system, electrons stand at a certain distance to each other so that coulomb repulsion is diminished. Therefore, exchange-correlation density functional is developed to include the inhomogeneity of the electron gas as a function of the interelectronic distance r' and the electron density, $\rho(r')$. In order to overcome Coulomb repulsion obstacle, an interaction potential is required to prevent electrons with the same spin from being close to each other, which is also known as exchange-correlation hole.

In the density functionals, electron-exchange and electron-correlation assumptions are tackled on an individual basis. Wrong assumptions are arised from the separation due to the fact that the known exact form of the exchange operator (from the HF theory), is not identical with the exchange operator for a homogeneous electron gas [18]. The exchange and correlation density funtionals are improved by the implementation of previous parametrization of these model to obtain different observables determined from experiment and highly accurate HF calculations, such as reaction energies, vibrational spectra, atomization energies, etc. [18].

In the exchange and correlation functionals, the volume of the N electrons are defined by a regular grid where the electron density is evaluated in order to express it as a numerical value. Therefore, the electron density calculation along the grid fails when valence electrons are considered due to the contradiction between the exact electron density and the homogeneous electron gas approximation. Even though remarkable improvements are provided by the exchange-correlation functionals, the exact explanation of the self-interaction energy stems from Coulomb's repulsion between Kohn-Sham orbitals and the electron density could't be derived. One of the problems is that, the exchange-density functional is not totally capable of expressing the self-interaction in the uniform electron gas system due to the non-local nature of electron-exchange [17-19]. In order to overcome this obstacle, the combination of the non-local exchange operator from HF theory and exchange density functional is combined. The amount of HF exchange contribution is assigned depending on the accuracy of the calculation with respect to the data sets of experimental or high-level ab initio methods [18, 19]. The inclusion of HF exchange into the GGA and meta-GGA density functionals enables the calculation with high accuracy like it previosly provided by HF methods but with a reduced computational effort.

Since the exchange, v_X and correlation, v_C operators of the local density approximation (LDA), are not enough to express local exchange-correlation energy of the system, further knowledge of the local interaction of the Kohn-Sham orbitals with the electron density is introduced. In the exchange-correlation density functional, the improvement is achieved by the addition of the gradient of the electron density. While GGA functional include only the electron density and its first derivative, the meta-GGA functional includes second derivative of electron density additional to the density and its first derivative in the exchange correlation potential.

$$v_{XC} = \underbrace{E_{XC}[\rho(r')]}_{\text{LDA}} + \underbrace{\Delta E_{XC}[\rho(r'),\nabla\rho(r')]}_{\text{GGA}} + \underbrace{\Delta\Delta E_{XC}[\rho(r'),\nabla\rho(r'),\nabla^2\rho(r')]}_{\text{m-GGA}} \qquad (3.8)$$

GGA functionals have been improved to Hybrid-GGA and meta-GGA functionals. Hybrid density functionals have been developed with the combination of the exchange correlation of GGA with a percentage of HF exchange [20].

In this thesis, M06-2X hybrid functional is used, which is introduced by Zhao *et al.*

$$E_{XC}^{hyb} = \frac{X}{100} E_X^{HF} + \left(1 - \frac{X}{100}\right) E_X^{DFT} + E_C^{DFT} \tag{3.9}$$

In M06-2X functional, X is defined as 54, which is the percentage of Hartree-Fock exchange [21].

3.3. Basis Sets

A basis set is a set of one particle functions that is used to represent electronic wavefunction in density functional theory. Molecular orbitals are expressed as linear combinations of the atomic orbitals by LCAO-MO approximation.

$$\phi_i = \sum_{\mu=1}^{K} c_{\mu i} f_\mu \tag{3.10}$$

where the functions ϕ_i are molecular orbitals, f_μ are atomic orbitals and $c_{\mu i}$ are coefficients and K is the total number of atomic orbital functions.

Split-valence basis sets are introduced by Pople, in order to reduce the computational cost and they are widely used in computational chemistry. In this method, valence and core electrons of an atom are tackled with two different basis sets. A smaller basis set is used for the core electrons due to their higher stability to the enviroment whereas a larger basis set is used for the valence electrons. For instance, 6-21G, 6-31+G and 6-311G* are some of the common basis sets in which the functions are splitted. The numbers on the left hand-side of the dash shows the number of Gaussian functions for core orbitals and on the right hand-side for the valence electrons. Two numbers mean valence double-ζ basis, and three numbers

mean valence triple-ζ basis. In order to extend the basis set, polarization and diffuse functions can be added [22].

In Polarization functions, higher angular momentum is added to all heavy atoms and it is described by "*" (d). The polarization of hydrogen atoms are taken into account by the addition of "**" (d,p) into the function.

Diffuse functions are used to include an atom that is far from the core electrons into the system. Diffuse functions are denoted by the "+" sign to heavy atoms which allows orbitals to occupy larger spaces. Additional "+" sing denotes diffuse functions to hydrogen atoms.

3.4. Continuum Solvation Models

Continuum Solvation Models are used to include solvation effects into quantum mechanical calculations. The description of the system in a continuous way decreases the number of degree of freedom by the means of a distribution function [23, 24].

In continuum solvation models, a polarizable medium is used to represent the solvent in the system. The polarizable medium is defined by its static dielectric constant ε while the solute is embedded in a cavity surrounded by the dielectric medium.

The total solvation free energy is defined as,

$$\Delta G_{solvation} = \Delta G_{cavity} + \Delta G_{dispersion} + \Delta G_{electrostatic} + \Delta G_{repulsion} \quad (3.11)$$

where ΔG_{cavity} is the energetic cost of placing the solute in the medium. Dispersion interactions between solvent and solute are expressed as $\Delta G_{dispersion}$ which add stabilization to solvation free energy. $\Delta G_{electrostatic}$ is the electrostatic component of the solute-solvent interaction energy. $\Delta G_{repulsion}$ is the exchange solute-solvent interactons not included in the cavitation energy.

The central problem of continuum solvent models is the electrostatic problem described by the general Poisson equation:

$$-\vec{\nabla}\left[\varepsilon(\vec{r})\nabla\vec{V}(\vec{r})\right]=4\pi\rho_M(\vec{r}) \tag{3.12}$$

simplified to

$$-\nabla^2V(\vec{r})=4\pi\rho_M(\vec{r}) \text{ within } C \tag{3.13}$$

$$-\varepsilon\nabla^2V(\vec{r})=0 \text{ outside } C \tag{3.14}$$

where C is the portion of space occupied by cavity, ε is dielectric function, V is the sum of electrostatic potential V_M generated by the charge distribution ρ_M and the reaction potential V_R generated by the polarization of the dielectric medium:

$$V(\vec{r}) = V_M(\vec{r}) + V_R(\vec{r}) \tag{3.15}$$

The Polarizable Continuum Model (PCM) belongs to the class of polarizable continuum solvation models [25]. In PCM, the solute is embedded in a cavity defined by a set of spheres centered on atoms, having radii defined by the van der Waals radius of the atoms multiplied by a predefined factor (usually 1.2). The cavity surface is then subdivided into small domains (called tesserae), where the polarization charges are placed. There are three different approaches to carry out PCM calculations. The original method is called Dielectric PCM (D-PCM), the second model is the Conductor-like PCM (C-PCM) [26] in which the surrounding medium is modeled as a conductor instead of a dielectric, and the third one is an implementation whereby the PCM equations are recast in an integral equation formalism (IEF-PCM) [27, 28]. The IEF-PCM have been used in this study.

4. CYCLOPOLYMERIZATION OF STYRENE

4.1. General Approach to Cyclopolymerization Reaction of Bistyrenic Monomers

The accurate control over the sequence of monomeric units in polymerization reactions has aroused great attention due to its ability to provide materials with different physical properties. Several groups have recently proposed innovative strategies for controlling sequences in chain-growth polymerizations, through judicious adjustments of the chemistry and polymerization mechanisms for the monomers, in conjunction with engineering tools, such as time-controlled monomer additions [29].

With the increased demand for the design of innovative materials, cyclopolymerization has become an important procedure for the production of desired materials. The two functional groups with the different reactivities toward the propagation step allow the sequence control due to the alternation provided by the intra-intermolecular chain mechanism of cyclopolymerization [7, 29]. Alternating aromatic units with the opposite (p-rich and p-deficient) electronic character through cyclopolymerization can be particularly interesting, yet achievable given the opposite reactivities toward polymerization of their styrene derivatives [7]. The reactivity of styrene-based monomers is controlled by the cyclization reaction of efficient difunctional monomers. Difunctional monomers are linked by a tether group which directs styrene groups favoring cyclization via free radical polymerization reaction [14].

In the systems where malonate ester (M1), diphenyl-silyl-based (M2), (methyl)phenyl-silyl-based (M3) tethering groups are used, two styrene moieties are linked to the tethers to possess steric hindrance in order to keep two polymerizable structures in close proximity, thus to orient them during propagation [8].

4.2. Experimental Details

All the experimental studies regarding cyclopolymerization of monomer M1, M2, and M3 are performed by Dario Pasini *et al.* in The University of Pavia. The experimental research indicates the synthesis and the efficient cyclopolymerization of two new difunctional monomers containing two styrenic moieties tethered each other by diphenyl silyl (M2) and (methyl)phenyl silyl (M3) based protecting groups. The efficiency of the reactions is compared with the cyclopolymerization reaction of previously synthesized monomer (M1) with malonate ester tethering group (Fig. 4.1.).

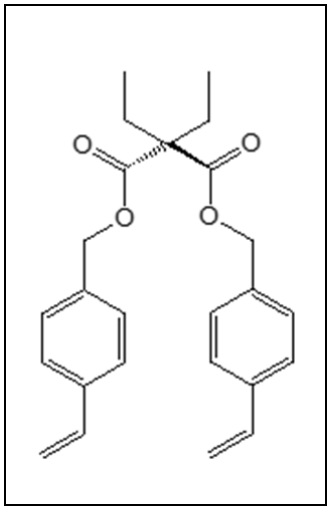

Figure 4.1. Bistyrenic monomer M1 with malonate ester tethering group.

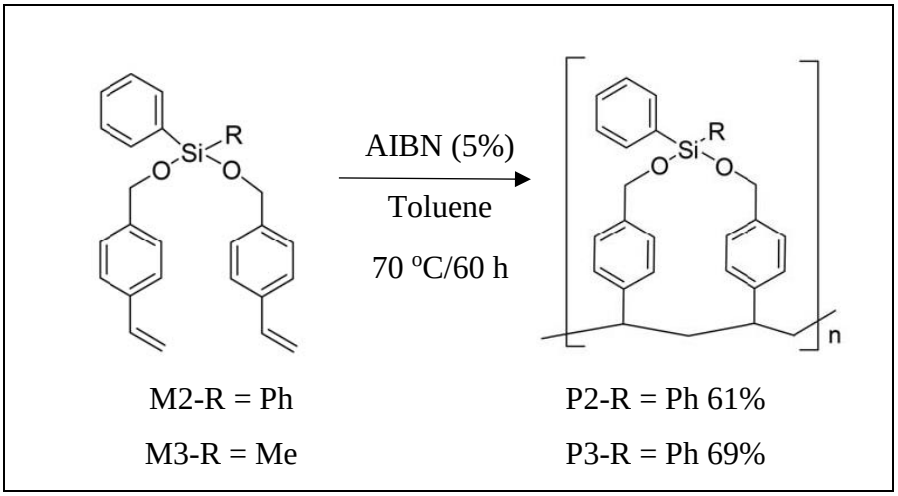

Figure 4.2. Synthesis of monomers M2 and M3.

Monomers M2 (diphenyl silyl-based) and M3 ((methyl)phenyl silyl-based) were synthesized through a similar reaction protocol, starting from 4-vinyl benzyl alcohol and either dichlorodiphenyl silane and dichloro-(methyl)phenyl silane. The nucleophilic substitution reaction was carried out in dry CH_2Cl_2 as solvent using an excess of 2,6-lutidine acting as the catalyst and as the base scavenger for the HCl generated from the reaction [8].

The siloxane-based tether groups have been selected on the basis of the following considerations: commercially availability, a good steric hindrance to favor the cyclization process during propagation and known procedures for the deprotection [8] and, hence, in the case of our cyclopolymerization systems, tether removal.

The new monomers were stable to silica gel and could be separated using flash chromatography, and obtained in a pure form in good yields (Fig. 4.2). Both monomers M2 and M3 were efficiently cyclopolymerized in toluene at 70^{o} C using a free radical initiator (AIBN) (Fig. 4.2). The polymerization reactions had to be carried out in high dilution conditions (monomer concentration in toluene 0.1 M), and with a relatively high percentage of AIBN (5%) to optimize yield and induce effective polymerization, in agreement with our previous reports with related systems [8, 14]. The mixture of reagents and products remained soluble during the reaction, with no apparent crosslinking, and cyclopolymers P2 and P3 were obtained in good yields (61% and 69%, respectively) after precipitation of the reaction mixture in MeOH as the nonsolvent. Whereas cyclopolymer P2 was soluble in common organic solvents, including THF for the GPC analysis, cyclopolymer P3 was only sparingly soluble in chlorinated solvents, and fully soluble only in toluene; therefore, in the latter case no GPC analysis could be performed. The GPC data for cyclopolymer P2 confirmed a good average degree of polymerization, essentially identical to that obtained from monomer M1.

The 1H-NMR spectra of the cyclopolymers polymers fully confirmed their proposed structures (Fig. 4.3), with the complete disappearance of the vinyl proton resonances, as to testify efficient cyclization, and the other significant proton resonances, as expected, broadened. The relative integration of the broad proton resonances area was in full agreement with the proposed structures and evidenced the quantitative presence of the tether units in the repeating unit of the macromolecular chains. Proton resonances of the 1,4-disubstituted benzene ring within the macromolecular backbone, appearing between 6 and 7

ppm, similarly to analogous systems [8] and polystyrene itself. The combined evidence of NMR spectra and solubility can be considered as a proof, as in previous cases, [8, 6] of the efficient mechanism that promotes perfect alternation of ring closure and propagation, avoiding the formation of crosslinked polymers.

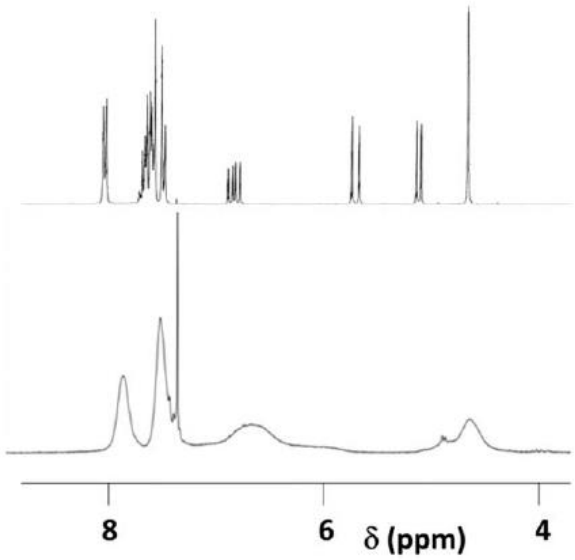

Figure 4.3. Comparison of 1H-NMR of monomer M2 (top) and cyclopolymer P2 (bottom).

4.2.1. Polymer Deprotection and Thermogravimetric Analyses

The deprotection step of the tethering group was attempted according to several methodologies (Fig. 4.4). Silyl ethers are widely utilized protecting groups, both for their ease of introduction on alcohol functionalities and for their stability in different mildly acidic or basic conditions. The most commonly used deprotection in the case of diphenyl silyl of phenylmethyl silyl groups is the use of fluoride ions. Attempts using n-Bu_4F in THF (in the presence of small amounts of H_2O) in combination with cyclopolymer P2 gave intractable solids.

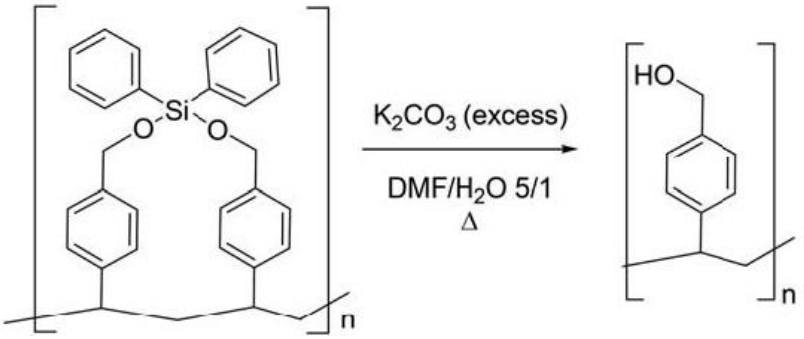

Figure 4.4. Tether removal from cyclopolymer P2.

The deprotection step of the tethering group was attempted according to several methodologies (Fig. 4.4). Silyl ethers are widely utilized protecting groups, both for their ease of introduction on alcohol functionalities and for their stability in different mildly acidic or basic conditions. The most commonly used deprotection in the case of diphenyl silyl of phenylmethyl silyl groups is the use of fluoride ions. Attempts using n-Bu_4F in THF (in the presence of small amounts of H_2O) in combination with cyclopolymer P2 gave intractable solids.

Experiments were then carried out on monomer M2, to verify efficient deprotection protocols, the deprotection affording known precursor poly(-4-strylmethanol), which could be detected simply by thin layer chromatography analysis. The most efficient deprotection protocol resulted to be in the presence of an excess of Na_2CO_3 or K_2CO_3, in THF/H_2O. Cyclopolymer P2 was thus subjected to similar deprotection conditions, using a different solvent mixture (DMF/H_2O) for solubility reasons, and reflux (100 ^oC) for 2 days; polymer poly(-4-strylmethanol) was isolated after an aqueous workup and extraction. The 1H-NMR spectra of the isolated polymer P2 (Fig. 4.4) was in agreement with the proposed structure.

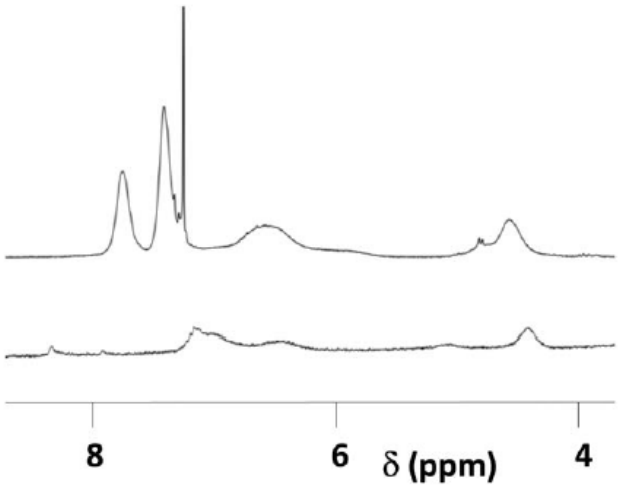

Figure 4.5. Comparison of 1H-NMR Spectra of cyclopolymer P2 (top), and poly(-4-strylmethanol) (bottom).

4.3. Computational Methodology

The ground-state geometries of the monomers M1, M2, and M3 and their derivatives have been optimized by the means of density functional theory (DFT). The long-range corrected M06-2X functional [21] along with the double zeta basis set 6–31G* has been used for the optimizations; transition state calculations are held at the same level of the theory. Transition states are characterized by a single imaginary frequency. To mimic the experimental conditions, the solvent effects were taken into account by utilization of the polarizable continuum model (PCM), in toluene environment at 343 K, 1.0 atm. All calculations have been performed with Gaussian 09 software package [30].

4.4. Results and Discussion

A conformational search around every single bond has been performed for monomers M1, M2, and M3 with the semi-empirical PM3 method. The most stable conformers have been optimized with M06-2X/6–31G* (around 15–20 conformers for each molecule within the range of 4 kcal/mol). The Gibbs Free Energies (M06-2X/6–31G*) for the structures corresponding to the stationary points along the initiation, cyclization, and propagation

reactions for M1, M2 and M3 are reported in Figure 4.6. The AIBN radical was used to initiate the free radical polymerization reaction for all the monomers M1, M2 and M3.

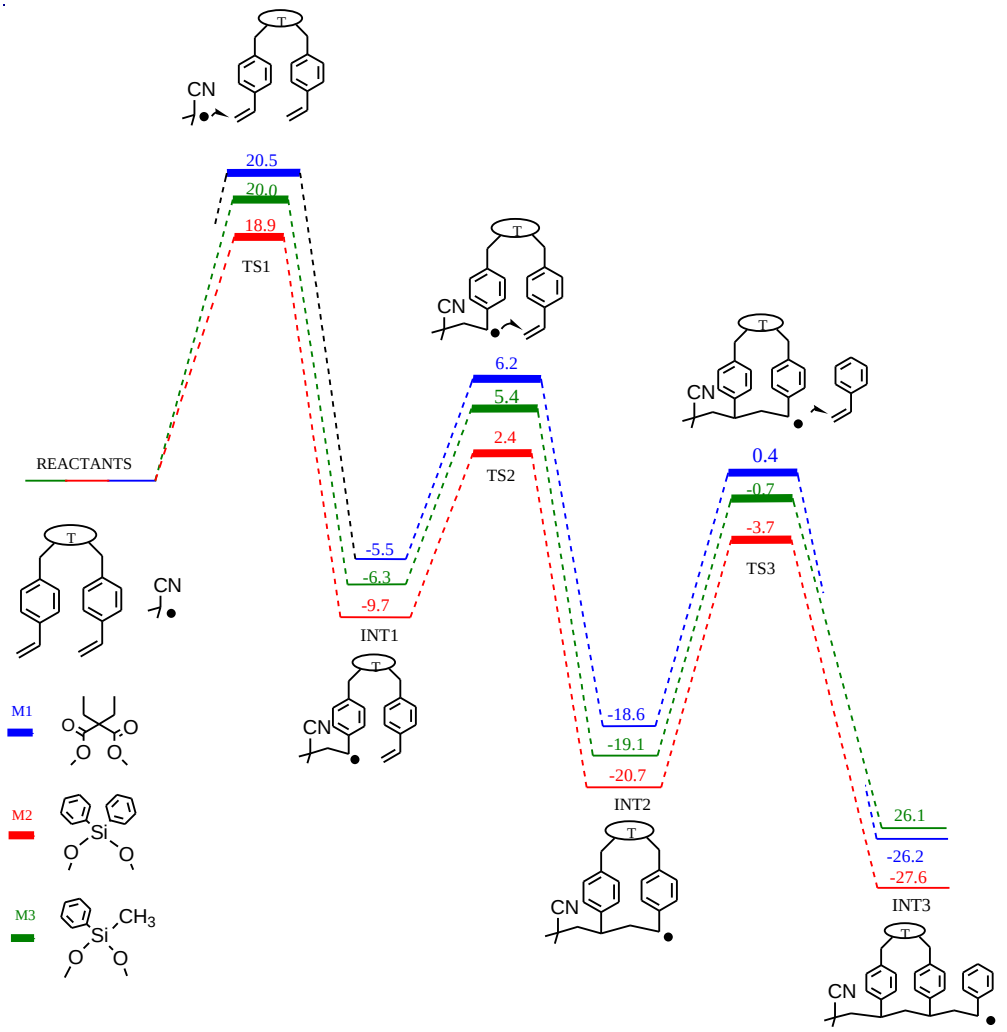

Figure 4.6. Gibbs free energy profile for the cyclopolymerization of M1, M2, and M3 (M06-2X/6-31G* in toluene at 70 ºC).

The 3D geometries of monomers, transition structures, and intermediate products are illustrated in Figure 4.6. Through the cyclization process, rearrangement of styrene groups is observed in a way that they get closer to each other. In the initiation step, the average distances between two styrene moieties within the monomers are 4.38, 3.75 and 3.73 Å for the first transition structures of M1, M2, and M3, respectively. Those distances in between

styrene groups become 3.93, 3.66 and 3.59 Å for the second transition state structures of M1, M2, and M3, respectively, in the cyclization process.

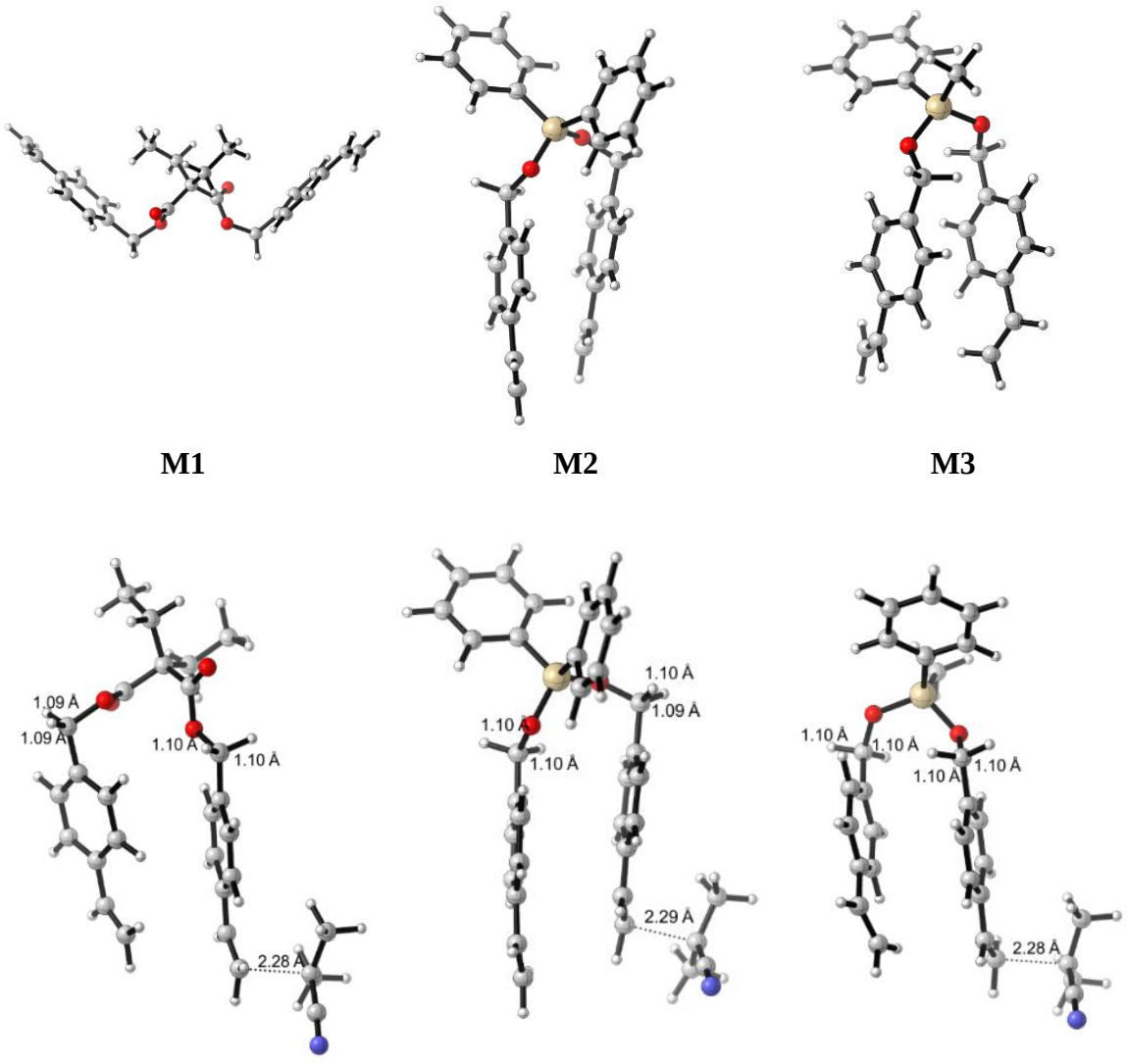

Figure 4.7. Optimized geometries for initiation, cyclization and propagation steps (M06-2X/6-31G*).

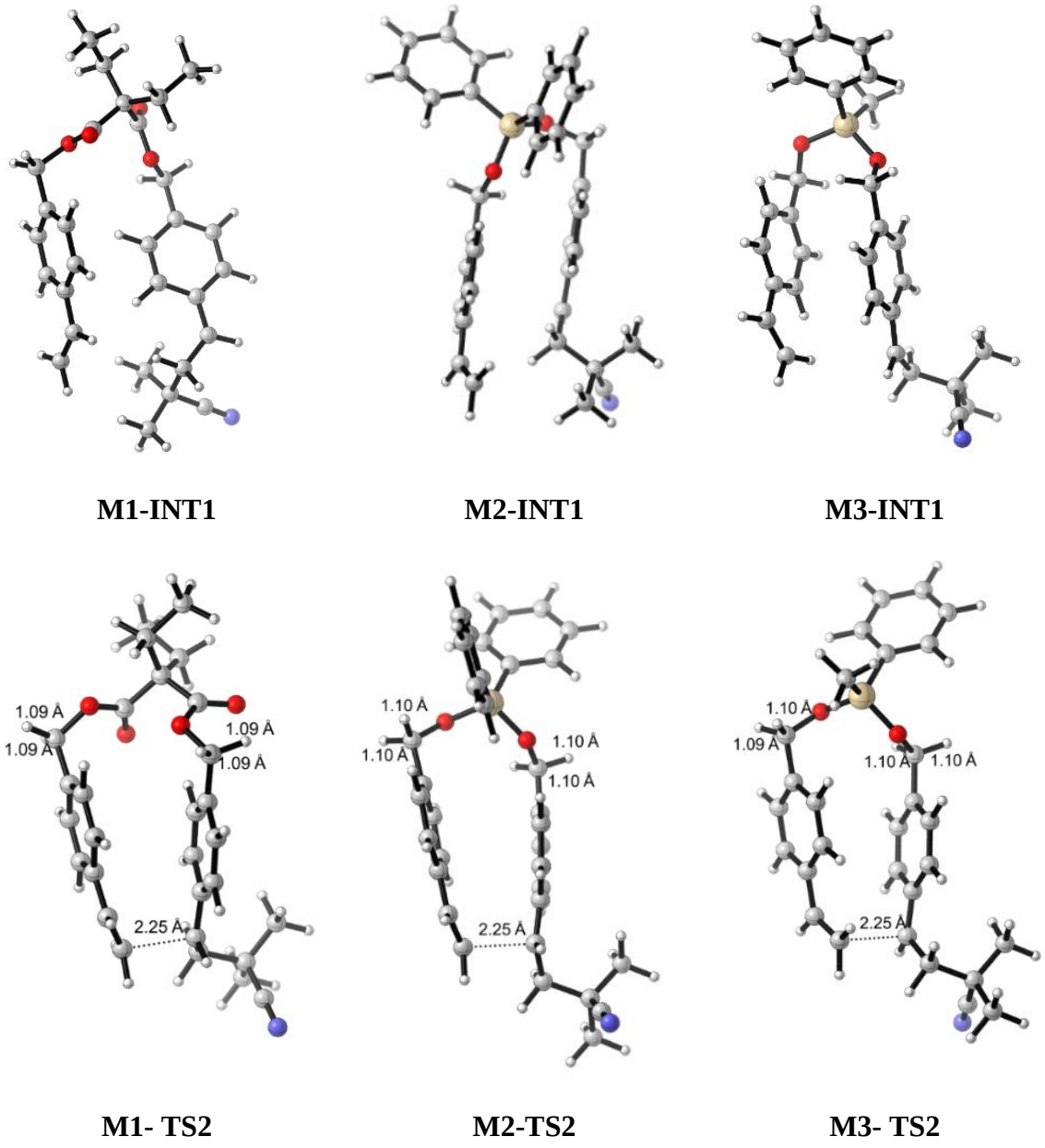

Figure 4.7. Optimized geometries for initiation, cyclization and propagation steps (M06-2X/6-31G*) (cont.).

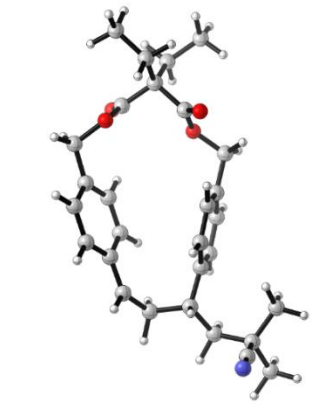

M1-INT2

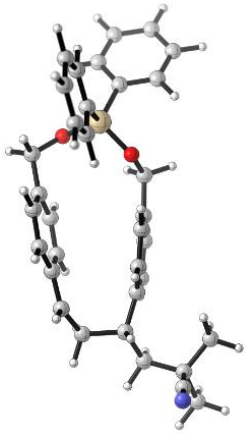

M2-INT2

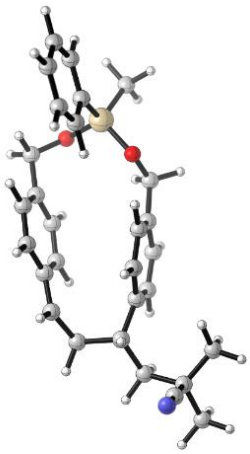

M3-INT2

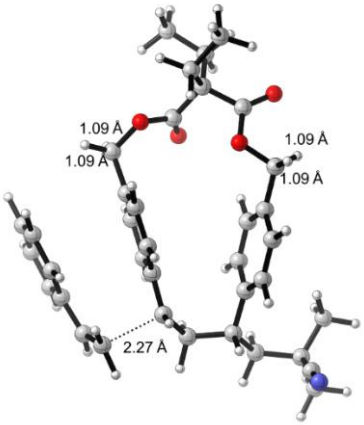

M1-TS3

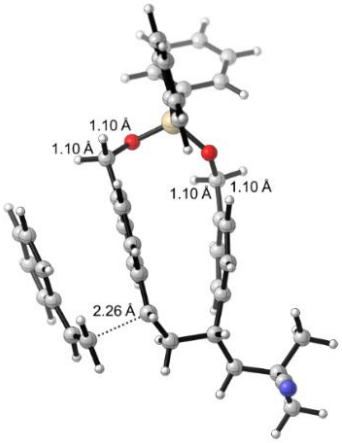

M2-TS3

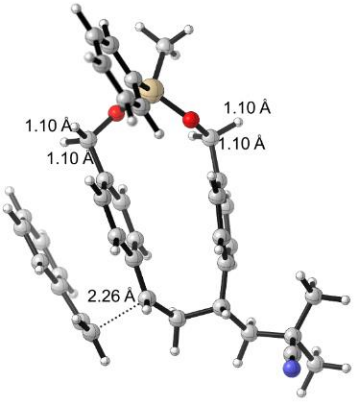

M3-TS3

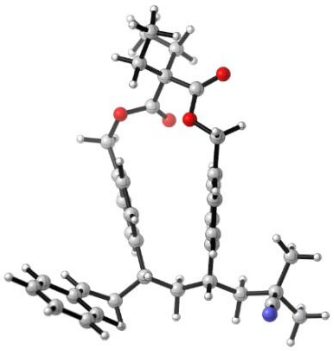

M1-INT3

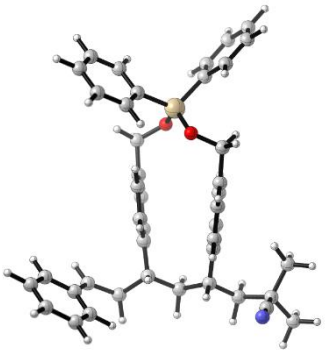

M2-INT3

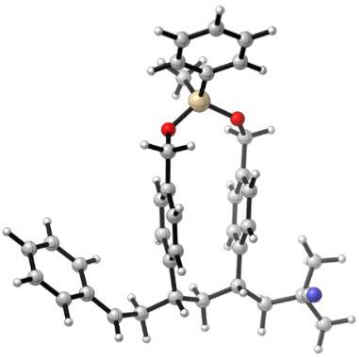

3-INT3

Figure 4.7. Optimized geometries for initiation, cyclization and propagation steps (M06-2X/6-31G*) (cont.).

The corresponding transition states (TS1) have barriers of 20.5, 18.9, and 20.0 kcal/mol and the critical distances are 2.28 Å, 2.29 Å, and 2.28 Å respectively. All these barriers are attainable at room temperature. The carbon radical center on INT1 is supposed to start the intramolecular cyclization via attack to the double bond. The cyclization via TS2 yielding INT2 is facile with overall barriers of 11.7, 12.1, and 12.0 kcal/mol, respectively, for M1-TS2, M2-TS2, and M3-TS2; the critical distance between the carbon radical and ethylenic carbon is 2.25 Å in every case. The intermediate INT2 initiates an intermolecular radical attack to another monomer. In this case, styrene has been chosen as a model for the second monomer. The barriers for TS3 starting from INT2 are 19.0, 17.0, and 18.4 kcal/mol with critical distances of 2.27 Å, 2.26 Å, and 2.26 Å for M1, M2, and M3, respectively. The propagation of the cyclic intermediate INT3 is also quite exoergic by -26.2, -27.6, and -26.1 kcal/mol for M1, M2, and M3. The 2D structures along the energy profile of the reaction are displayed in Figure 4.6. The 3D structures for the reactant, TS1, INT1, TS2, INT2, TS3, INT3 for M1, M2 and M3 are illustrated in Figure 4.7.

Modeling the initiation, cyclization, and propagation of M1, M2, and M3 has revealed the fact that these three reactions proceed in the same way without a considerable difference in the Gibbs Free energies for similar steps. In all three cases, the rate determining steps are the initiation and propagation steps, cyclization being more facile than the others.

The ease of cyclization can be attributed to the favorable attractive interaction between the aromatic rings. The Gibbs Free Energy of activation for M2 is lower in each step, hence the initiation, cyclization, and propagation steps of M2 is slightly more favorable than the corresponding steps of M1 and M3.

5. DENTAL ADHESIVES

5.1. Adhesion to Tooth

5.1.1. Structure of Tooth

The bulk of the tooth is composed of 30% collagen matrix and 70% high mineral hydroxyapatite content. The crown of the tooth has two main layers; dentin and enamel, which are biological hard tissues composed of calcium phosphate and collagen matrix. Enamel covers 1-2 mm of the upper layer of dentin, it contains 5% of collagen and 95% of hydroxyapatite [31]. Calcium phosphates are present as hydroxyapatite crystals and their principle storage are found in the form of $Ca_{10}(OH)_2(PO_4)_6$. Hydroxyapatite makes up the matrix of the teeth and provides rigidity [13].

Tooth decays are one of the major problems, which basically occur due to the deconstruction of enamel. Dental adhesive systems are improved in order to compensate the damage caused by enamel deconstruction and cavities in which bacterias enter and reach the root of the canal. In order to prevent such tooth damages, efficient bonding of adhesive systems to hydroxyapatite, the mineral component of enamel, is of interest. In the past, to obtain strong binding of monomers, acid etching technique was widely used to provide an irregular surface from very smooth enamel and to increase the interaction area [32]. However, with the discovery of self-etching monomers, an alternating and more useful technique has been brought to acid etching, therefore the damage of dentin by the external acid is prevented [10]. In this technique, monomers are improved in a way that they are able to etch the surface of the tooth and bind simultaneously by the acidic compartment of the monomers.

Various adhesive application techniques have been developed to recover the damaged surface of dentin. The generations of adhesives are defined depending on their effect on the changes in chemistry, the number of ingredients, bonding mechanism and their stability on the dentin surface. The recent improvements in the field as the seventh generation is the application of self-etching monomers, this does not require the technique-sensitive

rinsing step to eliminate phosphoric acid from enamel and dentin. The main purpose of the usage of self-etching monomers is to provide acidic and polymerizable components in the same molecule that etch and bond dentin or enamel simultaneously. General application of the self-etching adhesive systems includes two steps: the conditioning of enamel with the self-etching monomer and the treatment of an adhesive resin successively [10].

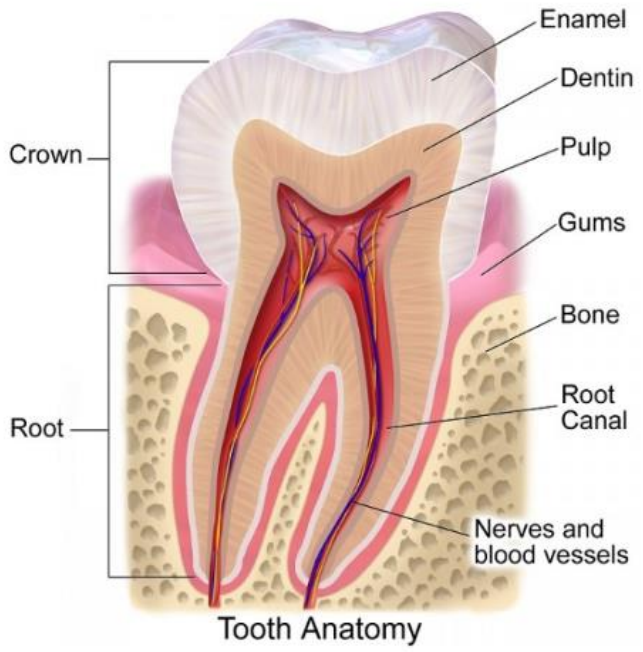

Figure 5.1. Structure of the tooth [33].

5.1.2. Self-Etching Adhesives

The commercial self-etching adhesives contain three main chemical groups; self-etching adhesive monomers, cross-linking monomers, additional monofunctional co-monomers, and additives such as initiators, solvents, stabilizers (Fig.5.2). In the self-etching adhesive systems, chemical groups are used to provide free radical polymerization, optimal solubility in aqueous medium, sufficient mechanical strength of the adhesive layer, low oral toxicity, stability against degradation by external factors such as oxygen, heat, light, and water.

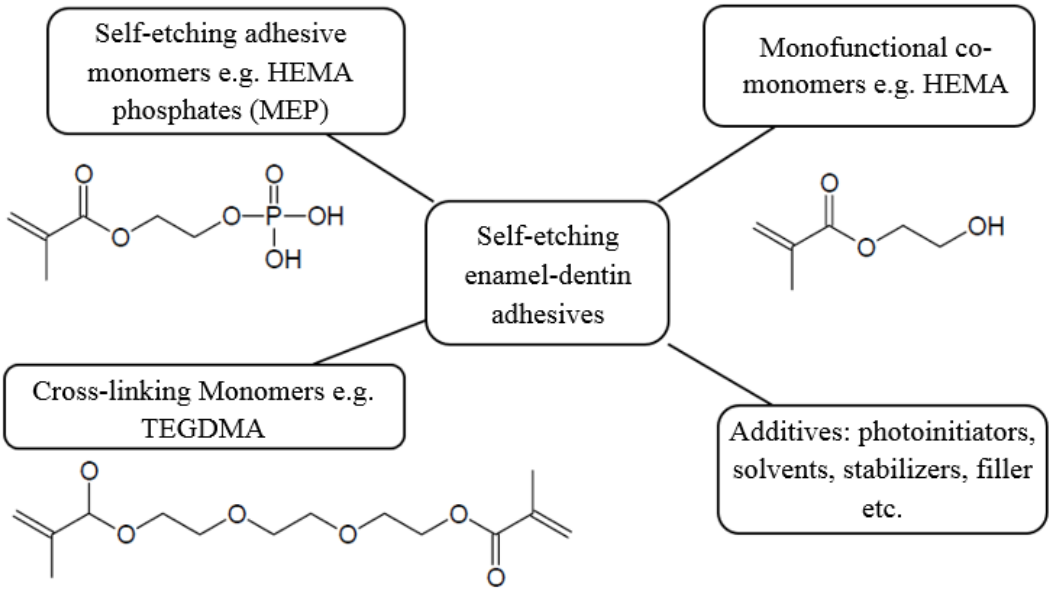

Figure 5.2. Components of self-etching adhesive systems [10].

The interaction of the adhesive mixture with the dental tissue takes place via the self-etching monomer component of the adhesive. Therefore, self-etching monomers are supposed to satisfy additional requirements such as being able to etch the enamel surface while forming micromechanical bonds on the surface, providing optimal wetting and capability of penetrating into the surface, fast ionic or covalent interaction with components of enamel or dentin. In order to provide these requirements, various self-etching monomers are developed. The common features of these monomers are having a polymerizable group P that reacts with the other crosslinking or monofunctional monomers and an acidic part AD which can etch the dental surface and interacts with hydroxyapatite component of dentin and having a spacer group R to control solubility, elasticity and wetting properties of the monomer [10].

In general, phosphorus-containing monomers such as phosphonic acids or acidic phosphates are widely used in self-etching adhesive systems. The stability of adhesives is provided by the strong interaction between the acidic group of monomers and calcium complex in hydroxyapatite. Monomer-calcium salts prevent hydrolysis with the electrostatic interaction [11]. On the other hand, charge transfer interactions, hydrogen bridges, Van der Waals and London dispersion forces have an impact on physical adhesion [10].

According to experimental studies, the effectiveness of the monomers can be managed by changing the spacer chains. It is asserted that the spacer chain affects the chemical interaction of monomer with hydroxyapatite. In order to test the bond strength, five standard-synthesized phosphoric-acid and three phosphonic-acid ester functional monomers with different spacer chains are used. The tested phosphoric-acid monomers are MEP and MTEP, CAP-P (intermediate hydrophilicity ester chain), MDP, MDDP (relatively hydrophobic ester chain) (Fig. 5.3), and phosphonic-acid monomers are HEAPA (two-carbon spacer chain with an acrylate end), EAEPA (two-carbon spacer chain with an ethyl-acrylate end), MEAEPA (two-carbon spacer chain with an trimethylphenyl-acrylate end) (Fig. 5.4) [11, 12]. The binding affinities of these phosphonic acid monomers are compared with that of MDP.

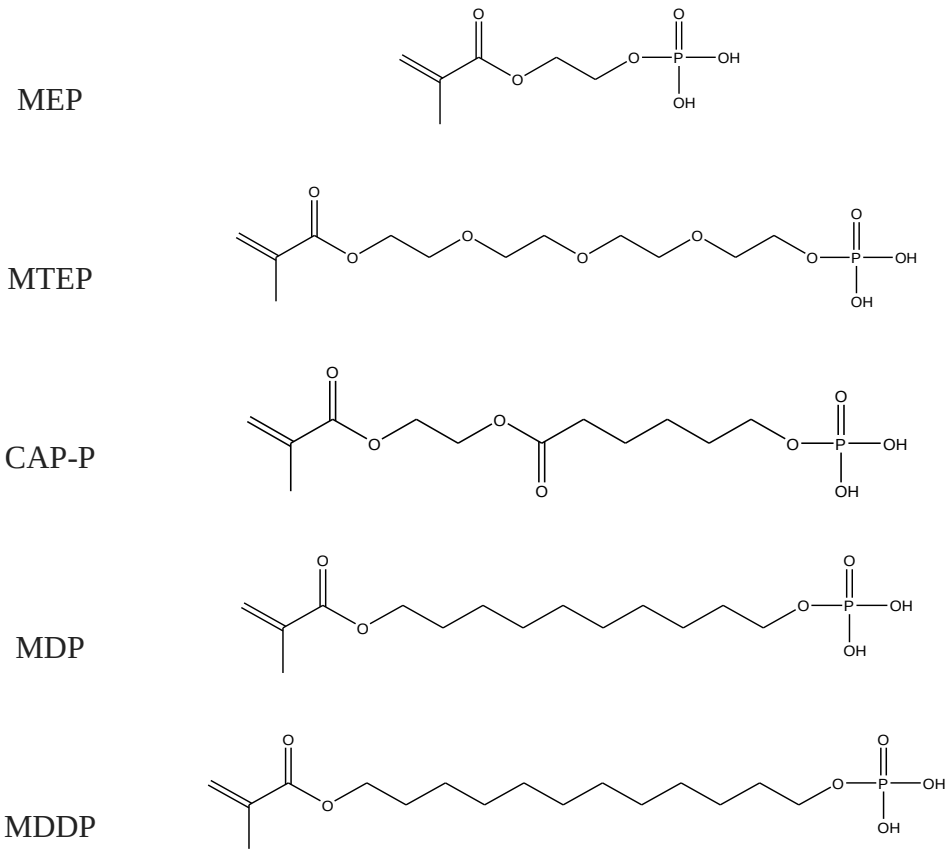

Figure 5.3. Phosphoric acid self-etching monomers.

HAEPA

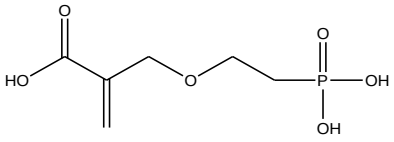

EAEPA

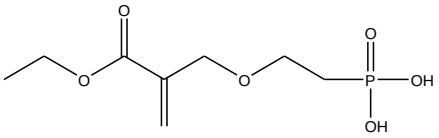

MAEPA

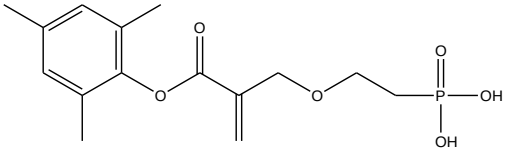

Figure 5.4. Phosphonic acid self-etching monomers.

5.1.3. Experimental Details of Functional Self-etching Monomers

In the previous experimental study of Yoshihara *et al.* [11], the chemical interaction and the bond strength of several self-etching monomers (Fig. 5.3) have been analyzed by atomic absorption spectroscopy (AAS), scanning electron microscopy (SEM), thin-film x-ray diffraction (TF-XRD), ATR-FTIR, and microtensile bond strength (μTBS). Salt formation with calcium is found in the order; MDDP>MDP>CAP-P>MTEP>MEP (Fig.5.5). FTIR and SEM analyses showed that monomer-treated dentin surfaces were resistant to rinsing for all monomer-dentin bonds, except with MEP (Fig. 5.6). The weaker interaction of MEP is stated by TF-XRD analyses. MDDP and MDP exhibited the highest μTBS values (Fig.5.7).

In the experimental study, AAS concentration of free calcium is calculated for the solution in which monomers are expected to precipitate by forming ionic bonds with free calcium ions, separately. The remaining calcium concentration is calculated showing that the lowest free calcium concentration refers to the highest percentage of precipitation. As a result, the lowest free calcium concentration is observed in the solution containing MDDP, which indicates its strongest binding affinity to calcium ion (Fig. 5.5).

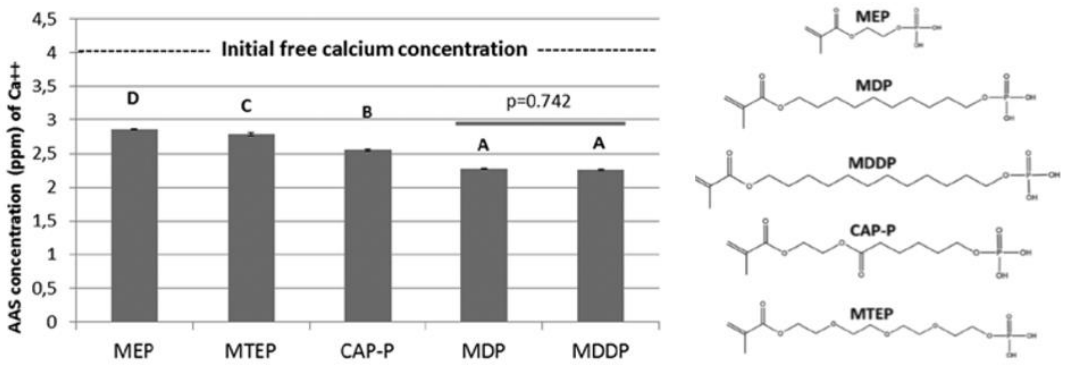

Figure 5.5. Free calcium concentration in the solution of calcium and monomers [11].

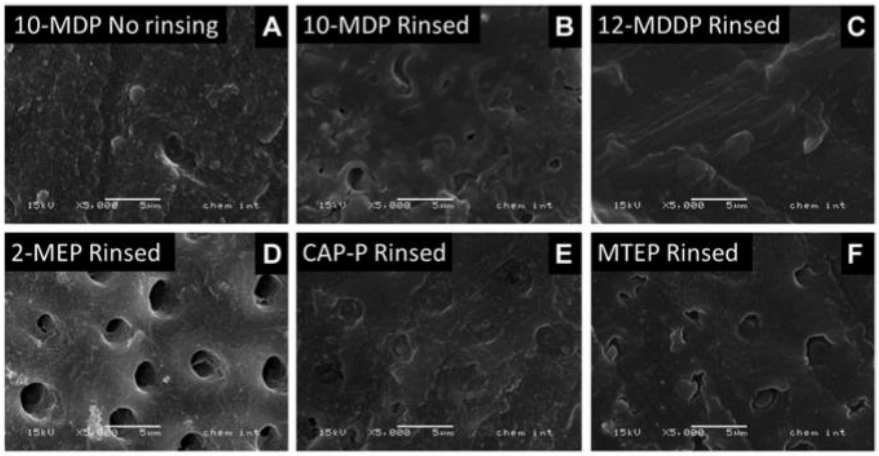

Figure 5.6. Scanning electron microscopy (SEM) micrographs showing the chemical interaction between self-etching monomers and dentin [11].

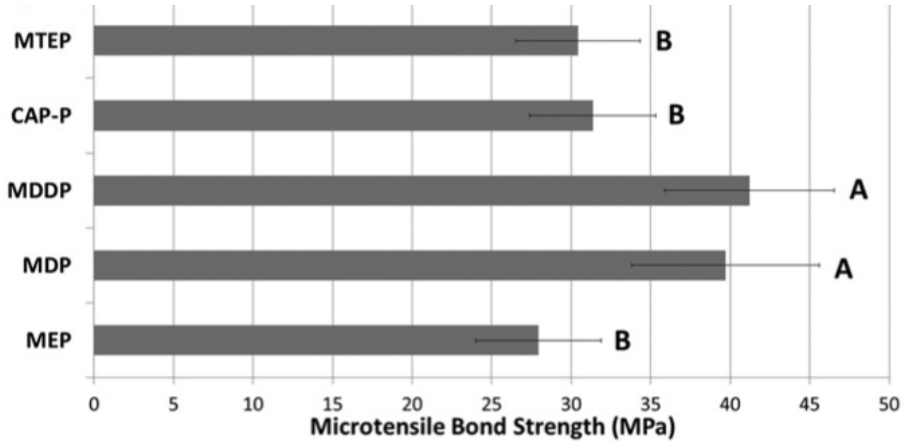

Figure 5.7. Microtensile bond strength test [11].

In another experimental study performed by Van Landuyt *et al.* [12], the phosphonate monomers (HEAPA, EAEPA, and MAEPA) are compared with MDP in order to illustrate how the small changes affect chemical bonding to calcium. The bonding capability is tested in terms of the microtensile bond strength of 4 types of cements (Fig.5.9).

AAS measurements evaluated the stability of the Ca-monomer salts, corresponded to the bond strengths of the 4 types of cements. The calcium salt of MDP exhibited the highest bond strength to enamel and dentin, hence, provided the highest stability (Fig. 5.8). Among the phosphonic acid monomers, the best overall bond-strength results were obtained by MAEPA. HAEPA salts are found hydrotically sensitive [12].

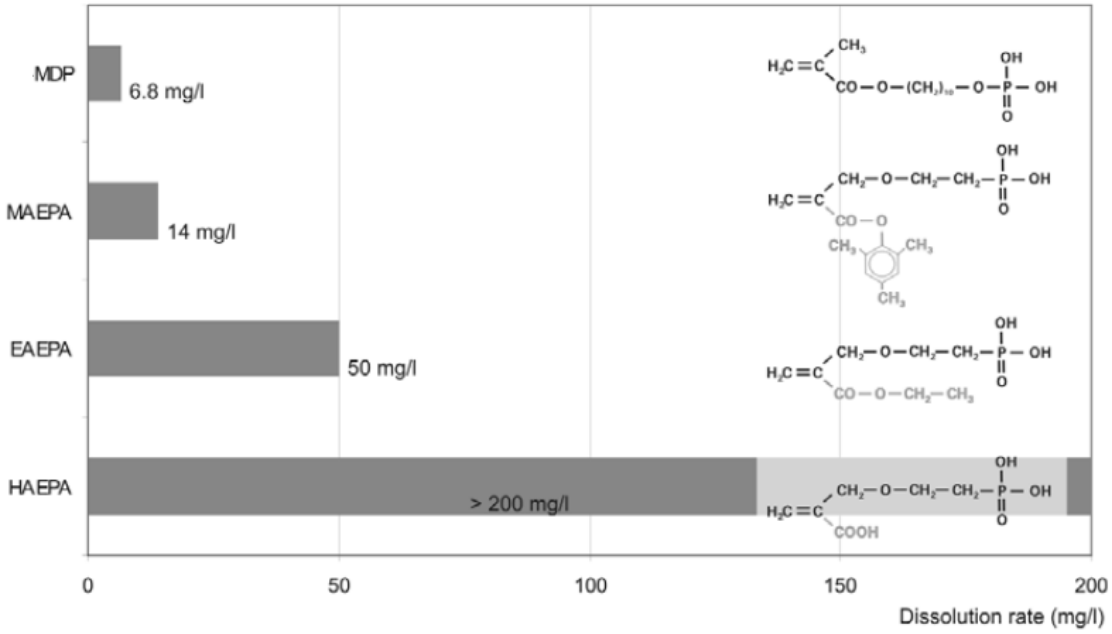

Figure 5.8. The dissolution rate of the calcium-monomer salts [12].

On the surface of the tooth, all HAEPA and the majority of EAEPA samples failed in binding before being tested. Conversely, MAEPA and MDP showed bond strengths of 25 MPa without pre-testing failures which means they have bonded to the surface efficiently (Fig.5.9). AAS measurements revealed that Ca-10-MDP salt was the most stable salt, followed by Ca-MAEPA and Ca-EAEPA. Ca-HAEPA was highly hydrolytically sensitive (Fig.5.8) [12]. Based on the experimental findings, the following ranking can be suggested

for the bond strength of monomers displayed in Figure 5.4: MDP > MAEPA > EAEPA > HAEPA.

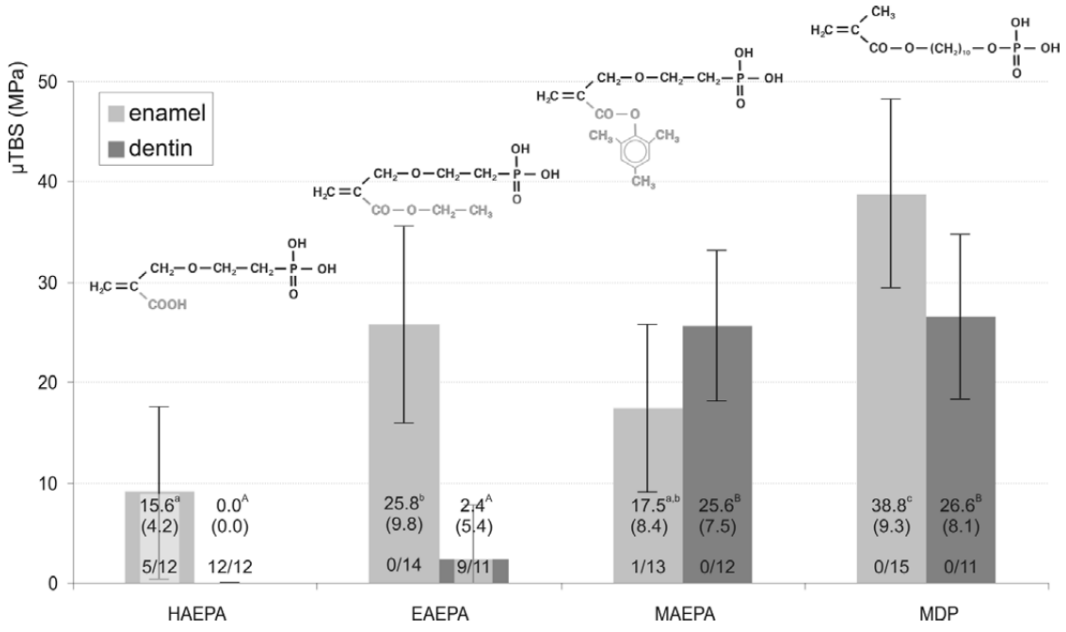

Figure 5.9. Microtensile bond strength of HAEPA, EAEPA, MEAPA, and MDP to enamel and dentin [12].

Since the driving force in this project is to model the monomer binding to calcium ion in hydroxyapatite content of enamel and analyze the binding efficiency of each monomer with computational tools, the pre-nucleation complex has been taken into account as a representative structure for hydroxyapatite.

5.2. Pre-Nucleation Complex

Hydroxyapatite with the formula $Ca_{10}(OH)_2(PO_4)_6$, is known as the major inorganic component of dentin and enamel, it originates from amorphous calcium phosphate structures in a process of dissolution and reprecipitation. In the past, calcium triphosphate complexes were identified as the key spherical structures that contribute to the formation of amorphous calcium phosphates (ACP). Free energy results obtained by umbrella sampling simulations [13] and several experimental studies by Habreken *et al.* [34] have shown that the 1:3 ratio

of Ca/P is the most energetically favored and more thermodynamically stable than the free ions.

In the 1970s, Posner's cluster is proposed with the formula $Ca_9(PO_4)_6$, suggesting that the cluster would aggregate randomly into larger ACP [35]. XANES and XRD experiments of the CaP precipitation stages suggests that the structural unit of ACP is the Posner cluster with the formula $Ca_9(PO_4)_6(H_2O)_{30}$. The cluster is thought to be formed by two deprotonated pre-nucleation complexes with the formula $[Ca(HPO_4)_3]^{-4}$ in which all the negative charges are compensated by calcium ions in the cluster [13].

The nucleation of ions is normally expected to occur by the packing of ions in the same way as small parts of the bulk crystal according to the classical nucleation theory. However, nonclassical nucleation theory assumes that initially stable pre-nucleation clusters form and they grow as they collide to form amorphous nanoparticles allowing ordered crystal phase eventually. Thus, the behavior of pre-nucleation complex and the details with their atomic structure has gain importance in order to shed light on the nucleation process of minerals. In the past, it has been shown that the driving force of the aggregation of highly charged solutes is the gain in entropy by the release of water and the formation of linear supramolecular polymers [36].

The nucleation process of calcium and phosphate ions are thought to be composed of several stages. It is supposed that the pre-nucleation complex is the transition state structure initiating the precipitation from free ions. In the study of Habraken *et al.* [34], precipitation of calcium phosphate has been presented in a buffered solution and under constant ionic strength. These wide ranges of in situ experiments such as AFM investigations, electron diffraction, and FTIR analysis have shown that the pre-nucleation clusters are calcium triphosphate complexes, which can aggregate into branched three-dimensional polymeric structures. Through the precipitation as spherical particles, aggregation and simultaneous binding of calcium to form amorphous calcium phosphates occur [34].

Habreken *et al*. has suggested the morphological development of amorphous calcium phosphate formation. According to their observations, after addition of phosphate solution to a solution of calcium ions, strands of nanometre-sized units appeared in the solution, and

they formed branched polymetric network which later transformed to nodules with dimensions of 150-200 nm and then spheres [34]. After 1h, those spheres transformed to ribbon-like morphology which evolved into elongated plates (Fig.5.10.).

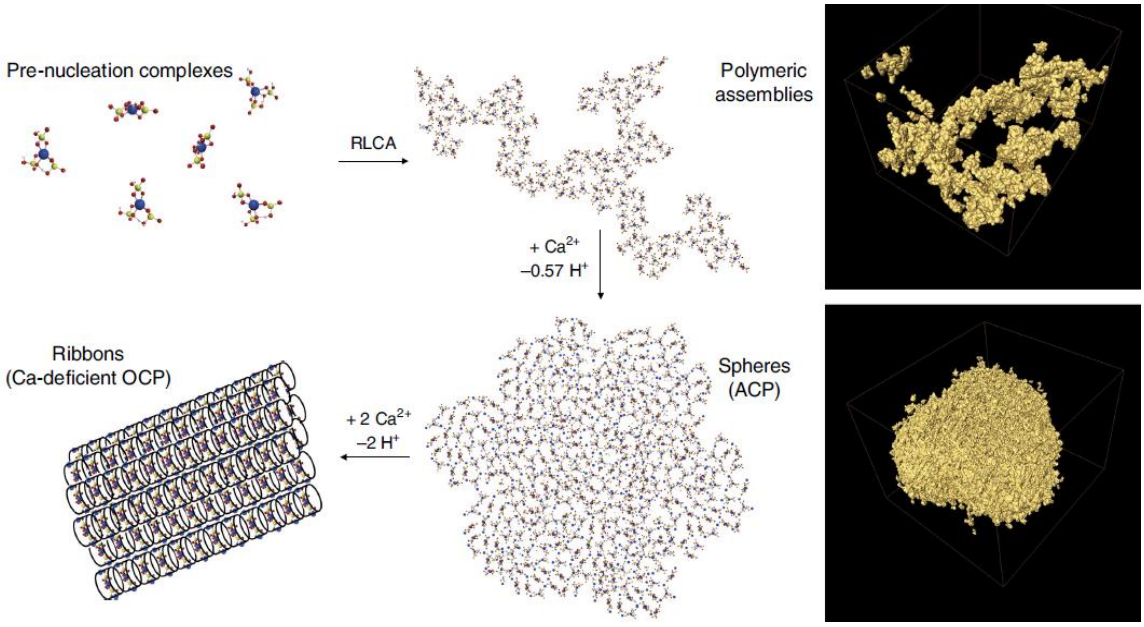

Figure 5.10. Calcium phosphate nucleation from pre-nucleation complex to form crystal phase [34].

Since the pre-nucleation complexes have been proposed, there has been no general agreement about the structure of most probable amorphous calcium phosphate formation due to the difficulty in accessing experimental information in such a small scale. However, there are a few studies in the literature concerning prenucleation complexes which lower the energy barrier to form hydroxyapatite crystals [13, 34]. Seven coordinated calcium triphosphate pre-nucleation complex including one water molecule has been shown by the ab-initio study of Habreken *et al.* (Fig. 5.11). It has been emphasized that the calcium triphosphate complex also forms the basis of the crystal structure of octacalcium phosphate and apatite [34].

A B

Figure 5.11. (a) 2D visualization of PNC proposed by Habraken *et.al.*, (b) Dimer of the pre-nucleation complex showing the potential of hydrogen bond formation. (Color key: Ca-blue, P-green, O-red, C-grey, H-white) [34].

In addition, the prenucleation complexes (PNC) with six and seven coordination number has been proposed by Manchardi *et al.* from University College London. In the study, pre-nucleation complexes have been analyzed by ab initio molecular dynamics (MD) simulations. According to their research, the most probably PNC is 7 coordinated with two water molecules containing calcium-triphosphate structure (II) (Fig.5.12) [13].

In the Molecular Dynamics study of Mancardi *et al.*, the $[Ca(HPO_4)_3]^{4-}$ PNC was optimized in the gas phase before the resulting structure was solvated with 93 water molecules using the Visual Molecular Dynamics (VMD) solvation tool in a cell of ∼15 × 15 × 15 $Å^3$. Neutralization of the -4 charge of the complex is provided by the addition two calcium ions. In the study, the system was first equilibrated in an NPT ensemble for 57.5 ps at a constant temperature of 300 K and 1 bar of pressure to regulate the density of water and then for a further 60 ps in an NVT ensemble (T = 300 K). The time step was set to 0.5 fs.

Throughout the molecular dynamics simulations, the coordination number of calcium ion has been taken into account. First of all, a structure with three bidentate phosphate groups are attached to calcium ion (I) has been optimized in the gas phase. Then, the simulations have shown that two water molecules also interact with calcium ion of PNC along with NVT dynamics and they enter the first solvation shell. The final structure has been illustrated as $Ca(\eta^2{-}\ HPO_4^{2-})_2(\eta^1{-}HPO_4^{2-})(H_2O)_2$ having a distorted pentagonal bipyramidal geometry.

Several conformations were obtained depending on the axial or equatorial positions of bidentate ($\eta^2-HPO_4^{2-}$) and monodentate ($\eta^1-HPO_4^{2-}$) phosphates.

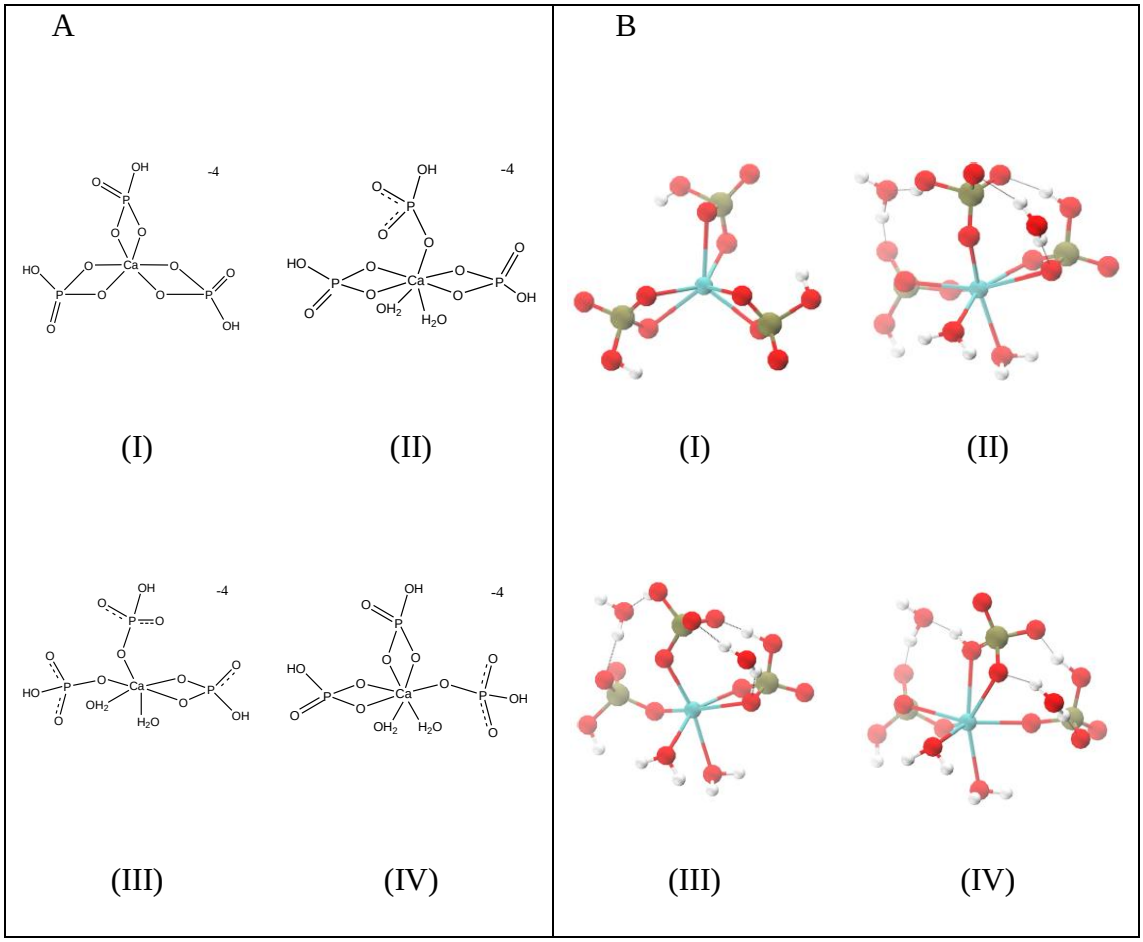

Figure 5.12. PNC I, II, III, IV (in water) from MD simulations [13].

As a result of the simulations, it has been proposed that complex II is more stable than complex IV after equilibration. The radial distribution functions obtained from the 60 ps of NVT trajectory shows that axial Ca-O_{ph}, Ca-O_{wat} pairs are located at 2.45 Å and 2.55 Å respectively. Almora-Barrios and de Leeuw reported Ca-O_{ph}, Ca-O_{wat} distances for various calcium phosphate complexes in water for the nucleation of hydroxyapatite as 2.2-2.6 Å and 2.4 Å, respectively [37].

The decrease in the positive charge of calcium ion due to -2 charge of phosphate groups is found to be the key factor for the presence of monodentate ligand. As the electrostatic interaction between calcium and phosphate decreases, hydrogen bonds with water molecules become more effective to have a monodentate position [13].

The stability of the calcium triphosphate complex in water has been evaluated through the analysis of free energy profile (Fig.5.13). The stability of the PNC II with respect to the free ions has been illustrated by the free energy calculation of the removal of the axial phosphate. The energy required to remove the axial phosphate in accordance with the entrance of third water molecule is found around 22 kcal/mol [13].

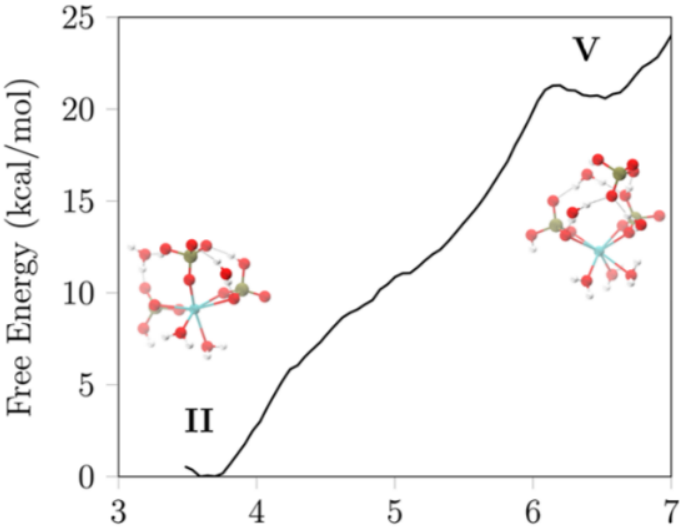

Figure 5.13. Free energy profile obtained by the removal of the axial phosphate group from PNC. Color key: Ca-cyan, P-green, O-red, H-white [13].

In the study of Mancardi *et al*., the 7 coordinated calcium triphosphate structure is found to be more stable than the free ions and its other derivatives [13]. However, since there is no general agreement between the structures of pre-nucleation complexes, we have decided to carry out a computational approach by density functional theory. Previously, Habraken *et al*. have emphasized that the kinetically stable PNC is expected to transform into the thermodynamically more stable one [34]. Thus, in our study, additional possible pre-nucleation complexes have been optimized in water and their electrostatic and zero-point energies have been calculated in order to obtain the most stable conformation of the PNC. Furthermore, additional possible coordination numbers of calcium ion in the complex has been analyzed. The previously proposed diffraction experiments suggested that the coordination number of calcium ion in aqueous solution varies between 6 and 8 [38].

Therefore, binding energy calculations for calcium water complexes are carried out to extend the scope of prenucleation complexes.

Additionally, Mancardi *et al*. have emphasized the energetic change within the complex when the axial phosphate makes monodentate type binding instead of bidentate type binding. During most of the MD simulations, it was observed that the axial monodentate phosphate remained in its position. The difference between the two binding patterns is shown in Figure 5.14. For this reason, in our study, the effect of the binding type of phosphates are investigated.

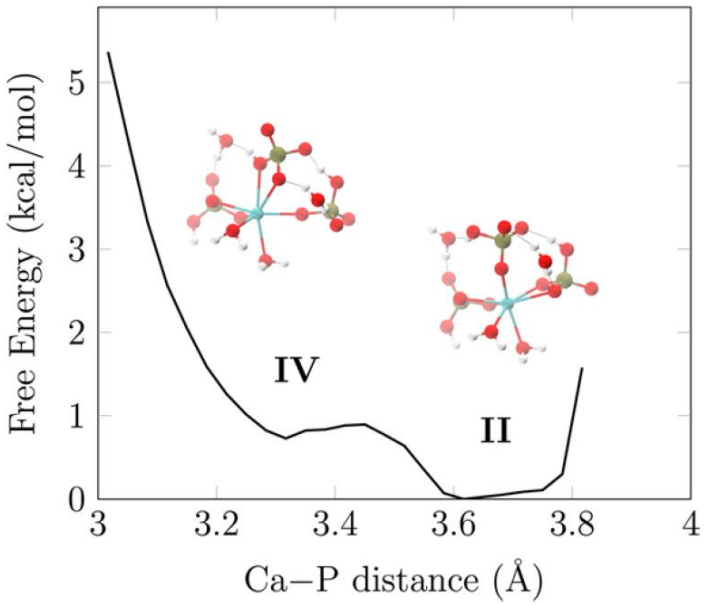

Figure 5.14. Free energy profile of PNC II and IV. (Color key: Ca-cyan, P-green, O-red, H-white.)

5.3. Computational Methodology

In this project, a conformational analysis for the self-etching monomers is carried out by using the semi-empirical PM3 method within the range of 5 kcal/mol difference. The ground state geometries of self-etching monomers such as MEP, MTEP, CAP-P, MDP, MDDP, EAEPA, MEAEPA, HEAPA, the pre-nucleation complexes and the monomer attached PNC's are optimized by the means of density functional theory (DFT). The long-

range corrected M06-2X [21] functional along with the double zeta basis set 6-31G** has been used for the optimizations in the water.

Several pre-nucleation complexes have been proposed with respect to their coordination number, binding type of the triphosphates and the number of water molecules. The formation and dissociation energies are calculated for each pre-nucleation complex. After determination of the most stable prenucleation complex, self-etching monomers have been bound to PNC at the axial position and the resulting complexes have been optimized at M06-2X/6-31G** level in water. Binding energies have been calculated in order to predict the strength of the interaction between hydroxyapatite and monomers.

5.4. Results and Discussion

In the literature, classical MD and DFT simulations indicated that calcium ion is capable of having a coordination number between 6-8 [39] [40]. In this research, the calcium-water complexes are optimized and their water binding energies are calculated in order to choose the most stable form of calcium-water complex for the following calculations.

$$[Ca(H_2O)_n]^{2+} \rightarrow [Ca(H_2O)_{n-1}]^{2+} + H_2O$$

$$\Delta E_b = E[Ca(H_2O)_{n-1}]^{2+} + E[H_2O] - E[Ca(H_2O)_n]^{2+}] \qquad (5.1)$$

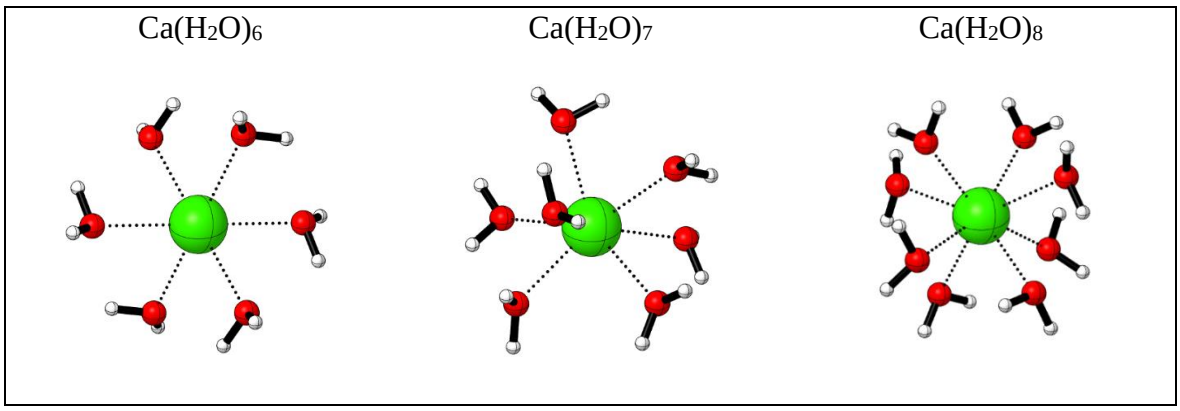

Figure 5.15. 3D geometries of Ca-water complexes in the gas phase (M06-2X/6-31G**).

Calculations by both Peschke *et al*. [41] and Bush *et al.* [42] indicate that $[Ca(H_2O)_5(H_2O)]^{2+}$ complex is approximately 5.25 kcal/mol higher in energy than $[(Ca(H_2O)_6{}^{+2}]$ with 6 CN structure where all the water molecules are coordinated to the central ion. Bruzzi and Stace *et al*. [38] applied the finite heat bath theory to kinetic energy release measurements in order to analyze water bindings up to 20 water molecules bonded to Ca^{+2} in the gas phase. The results suggest that the first solvation shell contains six water molecules. Also, they claimed that the 2+ charge on the calcium affects the molecular interactions which extend far beyond the first solvation shell.

The experimental work in which cross sections for the CID of the $Ca^{2+}(H_2O)_n$ complexes are measured using a guided ion beam tandem mass spectrometer, has been carried out by Damon R. Carl *et.al*., [43]. According to their results, the binding energies decrease monotonically from $Ca(H_2O)_5$ to $Ca(H_2O)_7$ whereas the binding energies of $Ca(H_2O)_7$, $Ca(H_2O)_8$, are very close to each other, differing by approximately 0.5 kcal/mol. This suggests that 7 and 8 coordinated calcium-water complexes have similar binding motifs [43]. As a result, they concluded that six water molecules bind directly to the calcium ion.

In this study, the water binding energies for $Ca(H_2O)_n$ complex where n is 6,7 and 8 are calculated in the gas phase with respect to equation 5.1. The results obtained from DFT calculations for water binding energies of $Ca(H_2O)_6$, $Ca(H_2O)_7$, $Ca(H_2O)_8$ are 32.7, 23,7, 22.9 kcal/mol, respectively. The results show that $Ca(H_2O)_6$ is more stable than its corresponding versions with 7 and 8 coordination numbers.

Even though 6 coordination number has been suggested for calcium-water complexes previously [44], and our results support the suggestions, it also has been stated that the coordination number of calcium is variable depending on factors such as concentration, pH, and temperature [43]. In this project, due to the variability of the coordination number of calcium ion, several calcium-triphosphate pre-nucleation complexes have been proposed in order to obtain the most stable form with respect to 6, 7 and 8 CN and different numbers of water molecules.

In the computational study of Mancardi *et al*., it is stated that the 7 coordinated $Ca(\eta^2{-}HPO_4{}^{2-})_2(\eta^1{-}HPO_4{}^{2-})(H_2O)_2$ pre-nucleation complex having 2 bidentate and 1

monodentate phosphates is energetically more stable when the monodentate phosphate is located in the axial position instead of the equatorial position (Fig.5.15) [13]. In this study, electronic and zero-point energies of pre-nucleation complexes in water are calculated. The same approach has been carried out by optimizing and comparing the similar structures of PNC II, IV [13] which are named as 7-M-2 and 7-B-2, respectively. According to the electronic and zero-point energy calculations, 7-M-2 is found 4.6 kcal/mol less energetic than 7-B-2 (Table 5.4). That indicates the energetic cost of the change in the position of the monodentate phosphate favoring the axial position.

The effect of the axial position of the complex in declining the energy was previously emphasized and a similar stability order is observed in our calculations. Therefore, in this study, the proposed pre-nucleation complexes are also categorized depending on the binding type of the phosphate groups at the axial position. 13 Prenucleation complexes with coordination numbers (6,7,8), different numbers of water molecules have been considered. Their binding properties have been analyzed. The nomenclature of the molecules indicated in Table 5.1 is assigned as follows;

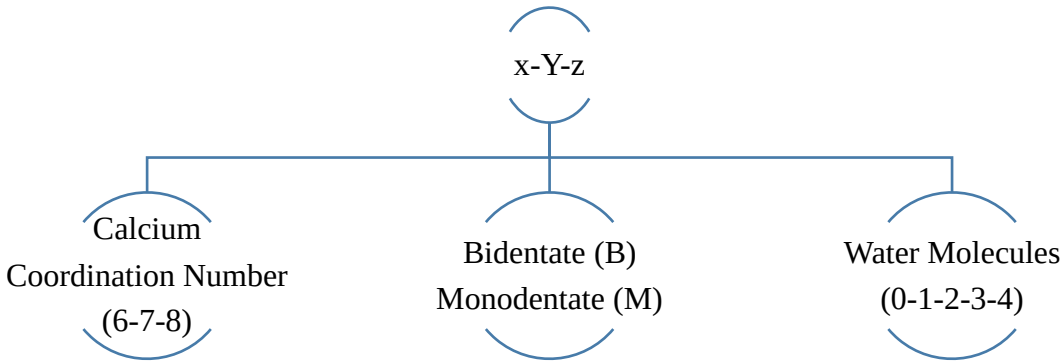

x represents the coordination number of calcium ion varying between 6-8, whereas Y represents monodentate (M) or bidentate (B) binding type of the axial phosphate groups and z indicates the number of water molecules in the first solvation shell. All the structures have three phosphate groups, one calcium ion having a different coordination number and different number of water molecules.

Table 5.1. Choice of pre-nucleation complexes with water.

CN/6	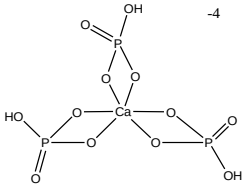	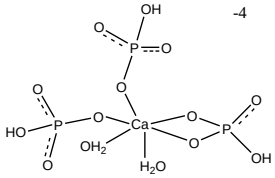	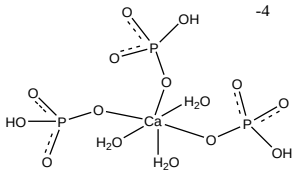
	6-B-0	6-M-2	6-M-3
CN/7	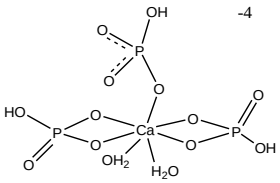	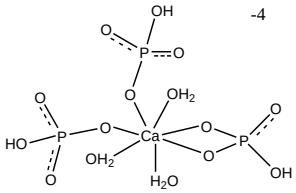	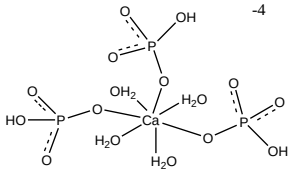
	7-M-2	7-M-3	7-M-4
	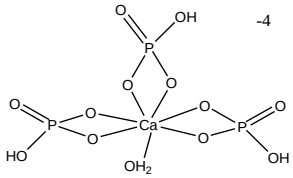	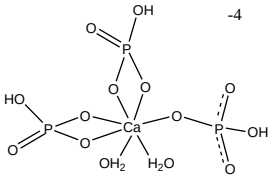	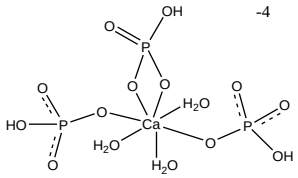
	7-B-1	7-B-2	7-B-3
CN/8		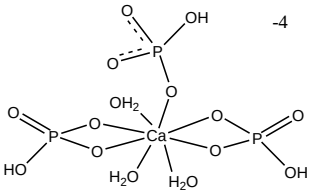	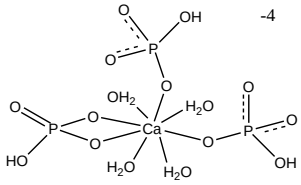
		8-M-3	8-M-4
	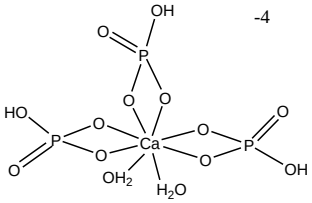	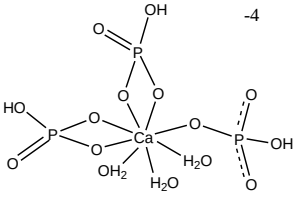	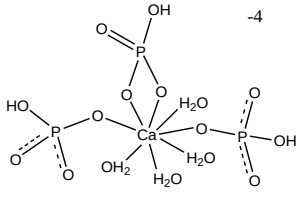
	8-B-2	8-B-3	8-B-4

Table 5.2. 3D illustration of optimized pre-nucleation complexes with water (M06-2X/6-31G** in water).

CN/6	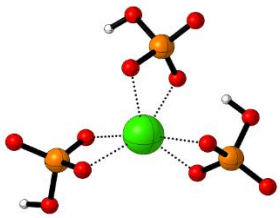	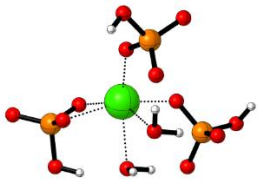	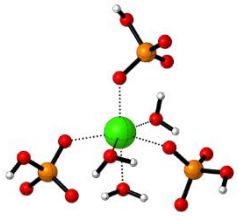
	6-B-0	6-M-2	6-M-3
CN/7	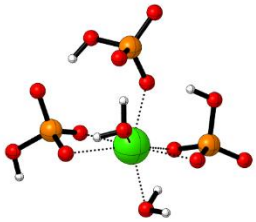	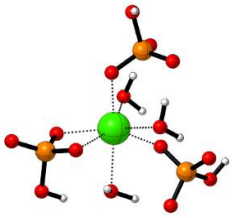	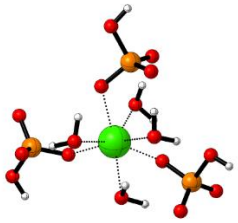
	7-M-2	7-M-3	7-M-4
	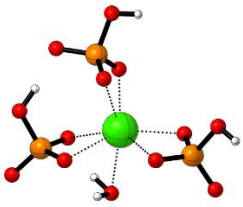	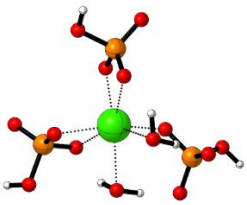	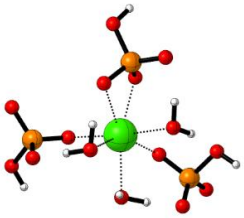
	7-B-1	7-B-2	7-B-3
CN/8		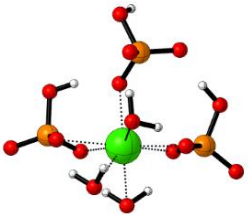	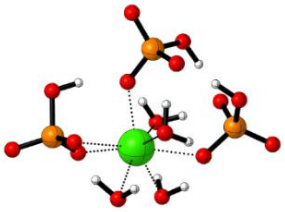
		8-M-3	8-M-4
	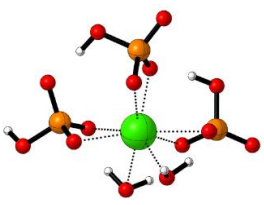	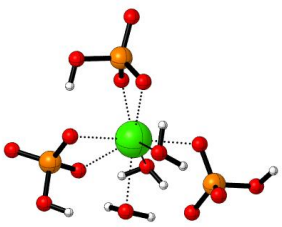	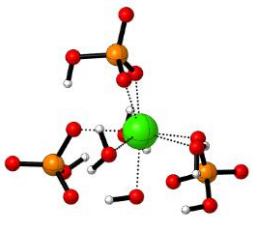
	8-B-2	8-B-3	8-B-4

5.4.1. Analysis of the PNC's

In the previous study, the structures I (6-B-0), II (7-M-2), III (6-M-2), IV (7-B-2) are proposed by Mancardi *et al*.[13]. During the MD simulations, it is observed that PNC I (6-B-0) has been transformed into calcium triphosphate complexes with 2 water molecules as the water molecules enter the first solvation shell. The free energy of II (7-M-2) is found to be 1.9 and 1 kcal/mol smaller than III (6-M-2), IV (7-B-2), respectively. In this work, (7-M-2) is found to be 5.3, 4.6 kcal/mol less energetic than (6-M-2) and (7-B-2), respectively (Table 5.4).

In order to decide about the most preferable prenucleation complex to analyze its interaction with self-etching monomers, their formation from $Ca(H_2O)_6^{+2}$ and $(HPO_4)^{-2}$ has been studied. The heat of reaction (ΔE_{rxn}) has been calculated for each complex by using equation 5.2 (Table 5.3).

$$[Ca(H_2O)_6]^{+2} + 3[(HPO_4)]^{-2} \rightarrow [Ca(HPO_4)_3(H_2O)_n]^{-4} + (6-n)\,[H_2O]$$

$$\Delta E_{rxn} = E_{el}[Ca(HPO_4)_3(H_2O)_n]^{-4} + E_{el}[(6-n)\,H_2O] - E_{el}[Ca(H_2O)_6]^{+2} - E_{el}[3(HPO_4)]^{-2} \quad (5.2)$$

The heat of reaction (ΔE_{rxn}) is taken into account to be able to compare the stability of previously proposed complexes. According to the calculations of the heat of reaction, (7-M-2) is found to be 33.8, 5.2, 4.5 kcal/mol smaller than (6-B-0), (6-M-2), (7-B-2), respectively (Table 5.3).

In the table 5.3, it is observed that the pre-nucleation complexes having the coordination number 8 have exhibited the lower heat of reaction values than the complexes with 6 and 7 coordinations. Among all the heat of reaction calculations for each pre-nucleation complexes, 8-M-4 is found energetically more favorable.

Table 5.3. Calculated heats of reaction (ΔE_{rxn}) for the formation of the pre-nucleation complex from calcium hexahydrate complex $(Ca(H_2O)_6)^{+2}$ and three phosphate ions $(HPO_4)^{-2}$ (M06-2X/6-31G** in water) (kcal/mol).

PNC	ΔE_{rxn}*	Rel [ΔE_{rxn}]
6-M-2	-99.5	45.0
6-M-3	-113.8	30.7
6-B-0	-70.9	73.6
7-M-2	-104.7	39.8
7-M-3	-118.3	26.2
7-M-4	-126.7	17.8
7-B-1	-60.0	84.5
7-B-2	-100.2	44.3
7-B-3	-109.9	34.6
8-M-3	-124.7	19.8
8-M-4	-144.5	0.0
8-B-2	-105.8	38.7
8-B-3	-120.8	23.7
8-B-4	-137.6	6.9

* $E = E_{electronic} + ZPE$

Location and Binding Mode of Axial $(HPO_4)^{-2}$ Group

In the following step, the location and binding modes of the phosphate ligands has been rationalized. When the complexes that have the same coordination number, the same number of water molecules, differing by binding type of the phosphate groups are compared, it has been observed that the monodentate phosphate groups are more favorable than the bidentate phosphates at the axial position. The axial phosphates of the complexes with the coordination number 6,7, and 8 have shown similar tendency to make monodentate bindings to the calcium ion. For instance, the energy differences between 7-M-2 & 7-B-2, 7-M-3 & 7-B-3, 8-M-3 & 8-B-3, 8-M-4 & 8-B-4 are 4.6, 8.3, 3.8, 6.9 kcal/mol respectively, favoring the monodentate phosphate at the axial position in each cluster.

In order to decide about the factors affecting the stability of the conformations of several pre-nucleation complexes, they have been categorized depending on the number of water molecules they have (Table 5.4). Thus, it is perceived that the complex 8-M-4 is energetically more favorable among the other complexes having 4 water molecules such as 7-M-4 and 8-B-4. Also, among the complexes having 3 water molecules attached to calcium ion, 8-M-3 is found more stable than 6-M-3, 7-M-3, 7-B-3 and 8-B-3. As it is expected, 8-B-2 has shown lower energy than that of 6-M-2, 7-M-2 and 7-B-2.

Table 5.4. Relative energies (electronic and zero-point) and dissociation (E_d) of pre-nucleation complexes, (kcal/mol), (M06-2X/6-31G** in water).

Complex	Relative [E][a]	[E_d][b]	Relative [E_d]
6-B-0	0.0	38.5	0.0
7-B-1	0.0	40.7	0.0
6-M-2	6.4	36.1	13.6
7-M-2	1.1	41.3	19.1
7-B-2	5.7	22.2	0.0
8-B-2	0.0	42.4	20.2
6-M-3	10.8	35.7	19.8
7-M-3	6.4	40.1	24.2
7-B-3	14.7	15.9	0.0
8-M-3	0.0	46.5	30.6
8-B-3	3.8	42.7	26.8
7-M-4	17.8	33.7	0.0
8-M-4	0.0	51.5	17.8
8-B-4	6.9	44.5	10.8

[a] Relative electrostatic + zero-point energies of the complexes.

[b] Dissociation energy of the complexes using the electrostatic + zero point energies.

These comparisons have shown that the complexes having the coordination number 8 are energetically more favorable than their other conformations having the same formula. Thus, further investigations were required to assess the differences in the complexes and the factors affecting their stability.

Since our main goal is to analyze the interaction of self-etching monomer with the most stable prenucleation complex, the energy required for the removal of the axial phosphate group is calculated for each complex so that the most stable conformations can be inferred. Thus, we have calculated the dissociation energies (E_d) for the removal of the axial phosphate groups in order to examine the stability of the PNC's.

$$[Ca(HPO_4)_3(H_2O)_n]^{-4} \rightarrow [(HPO_4)]^{-2} + [Ca(HPO_4)_2(H_2O)_n]^{-2}$$

$$\Delta E_d = E_{el}[Ca(HPO_4)_2(H_2O)_n]^{-2} + E_{el}[(HPO_4)]^{-2} - E_{el}[Ca(HPO_4)_3(H_2O)_n]^{-4} \qquad (5.3)$$

Among all the groups having the same structural formula (Table 5.4.), the dissociation energies for the removal of axial phosphate, E_d, is calculated. It is observed that the dissociation energy required for the removal of the axial phosphate group is found to be the highest in 8-M-4 (51.5 kcal/mol) among other structures (7-M-4 and 8-B-4). This result indicates the higher stability of the complex 8-M-4 among its conformers. Also, the highest dissociation energies in the groups having 3 and 2 water molecules in the complex have been found as 46.5 and 42.4 kcal/mol for 8-M-3 and 8-B-2, respectively.

In Table 5.5., the distance between the oxygen atom of the axial phosphate groups and calcium ion for each PNC is given. It is reported that the monodentate binding type causes slightly shorter calcium-oxygen distance compared to the bidentate binding type in the complexes having the same structural formula. It is also observed that, as the coordination number and the number of water molecules increases, the Ca-O distances also increases.

Table 5.5. Distance (Å) between Ca and O atom of the axial phosphate group.

PNC	d_{Ca-O}
6-M-2	2.30
6-M-3	2.29
6-B-0	2.39/2.44
7-M-2	2.32
7-M-3	2.35
7-M-4	2.41
7-B-1	2.41/2.48
7-B-2	2.41/2.46
7-B-3	2.45/2.60
8-M-3	2.35
8-M-4	2.37
8-B-2	2.45/2.40
8-B-3	2.39/2.47
8-B-4	2.40/2.42

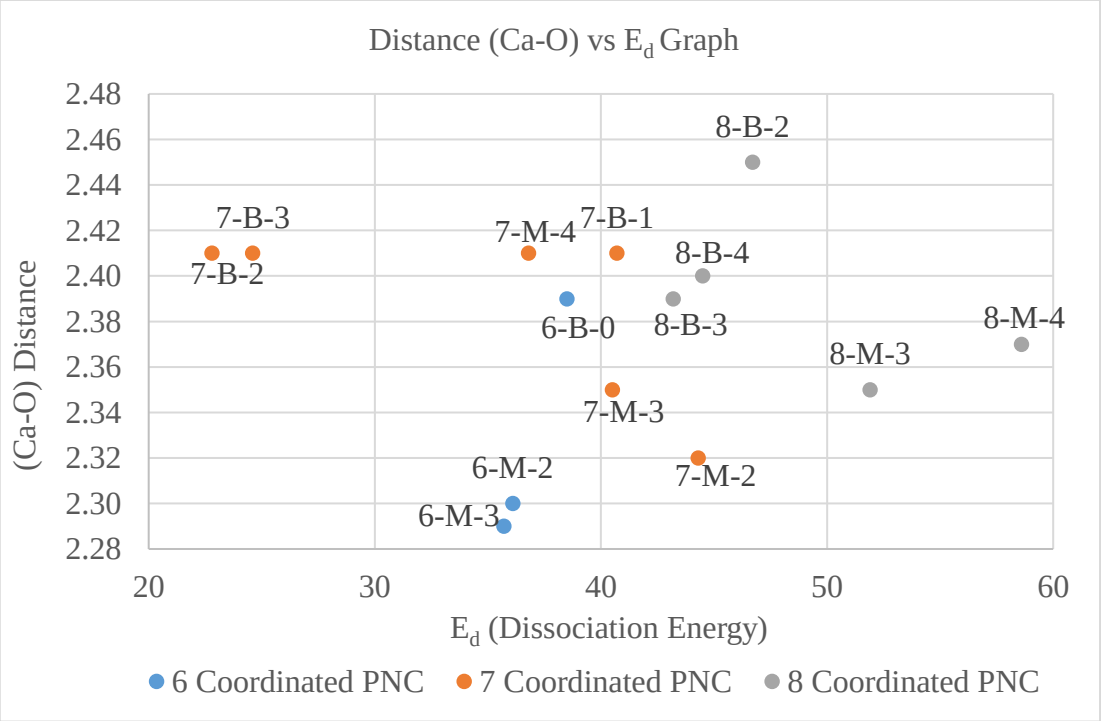

Figure 5.15. Ca-O (axial phosphate) distance (Å) vs dissociation energy (kcal/mol) (M06-2X/6-31G** in water).

The dissociation energy of the axial phosphate and the Ca-O distance graph (Fig. 5.15) shows that complexes with 8 coordination and monodentate axial phosphate binding type have higher dissociation energies (E_d) indicating higher stability of the complexes in which Ca-O distances are found slightly shorter than their versions having the same amount of water molecules or bidentate binding type.

Table 5.6. Hydrogen bonding distance (Å) of axial and equatorial phosphates with water molecules.

PNC	Axial Phosphate	Equatorial Phosphate
6-M-0		1.75 (ph)*
6-B-2	1.53	1.74 /1.88 1.51
6-B-3	1.55	1.72 / 1.73 1.63 / 1.66
7-M-2	1.51 1.69 / 1.66 (ph)*	1.64 / 1.85 2.29
7-M-3	1.62 1.68	1.72 /2.13 1.51 / 1.94
7-M-4	1.64 / 1.61 1.89	1.85 / 1.55 1.85 / 1.54
7-B-1	1.69 ph	1.8 2.08
7-B-2	1.85	1.63 / 1.85 1.66
7-B-3	1.77 1.82	1.82 / 1.53 1.52
8-M-3	1.58 1.61 / 1.78 (ph)*	1.80 /1.72 1.75 / 1.80
8-M-4	1.60 1.59 /1.60 /1.76(ph)*	1.56 / 1.59 1.75/ 1.97
8-B-2	1.63 (ph)* 1.74 (ph)*	1.52 /1.75 (ph)* 1.79
8-B-3	1.77 (ph)* 1.89	1.76 / 1.77 / 1.91 1.66 /1.85 / 2.15
8-B-4	1.71 (ph)* 2.10 / 1.88	1.89 / 1.99 /1.81 / 1.74 1.61 / 1.59 / 1.49

* (ph) indicates the hydrogen interaction with another phosphate group.

In addition, as the number of water molecules increases in each group having the same coordination number, a decrease in heat of reaction is observed indicating the increased stability of the complex (Table 5.3). Therefore, in order to further understand the effect of water molecules, the number of intramolecular hydrogen bonding is analyzed.

According to the results obtained from Table 5.3, the increase in the number of hydrogen bonds made by water molecules in the first solvation shell increases the stability of the complex. Thus, the complexes that exhibit higher stabilities have more intramolecular hydrogen interaction. As can be seen from Table 5.6, when the coordination number increases in prenucleation complexes, the number of hydrogen bonds also increases leading to higher stabilities. Although we have seen the effect of hydrogen bonds in the complexes having the same coordination number and the same type of axial phosphate binding which vary only with the number of water molecules such as 7-M-2,7-M-3,7-M-4 very clearly, the hydrogen bond effect is not high enough to compensate the effect of the monodentate binding type of the axial phosphate group. For instance, 8-M-4 and 8-M-3 are the most energetically favorable structures in their groups, however, even though their conformers 8-B-4 and 8-B-3 have the larger number of hydrogen bonds compared to 8-M-4 and 8-M-3, the effect of hydrogen bonding is not enough to render bidentate groups to an energetically more stable form. The complexes 8-M-4 and 8-M-3 are favored over their axial bidentate counterparts despite the higher number of intramolecular hydrogen interactions in the bidentate complexes. As a result of analyses, the effect of the coordination number (8) is found to be the most powerful criteria for the stability of the prenucleation complex.

5.4.2. Modeling Self-Etching Monomer Binding to Pre-nucleation Complex

The conformational analysis has been carried out for the phosphoric and phosphonic acid self-etching monomers by using the PM3 method within the range of 5 kcal/mol. After performing optimizations for the monomers (M06-2X/6-31G**), the conformations having the lowest electronic and zero-point energies have been chosen for the following analysis.

Table 5.7. 3D and 2D illustrations of self-etching monomers (M06-2X/6-31G** in water). (Color key: Ca-green, P-orange, O-red, C-grey, H-white).

Phosphoric Acid Monomers		Phosphonic Acid Monomers	
MEP	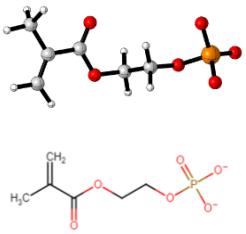	MAEPA	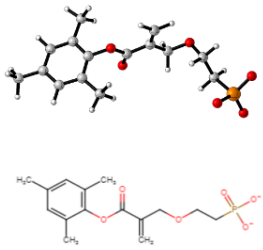
MTEP	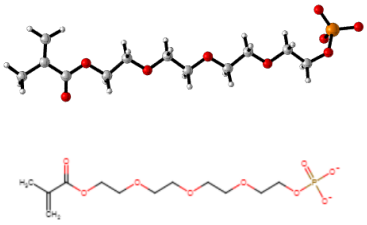	EAEPA	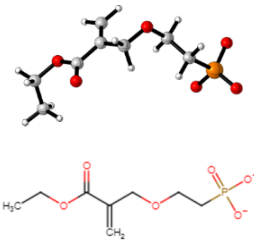
CAP-P	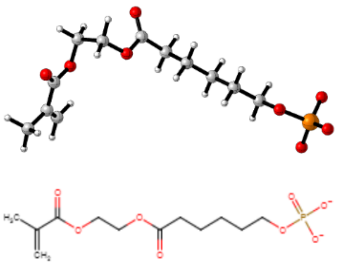	HEAPA	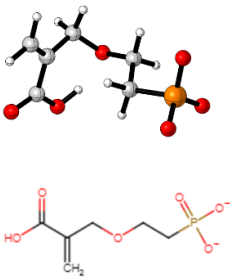
MDP	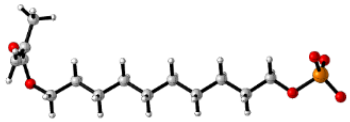		
MDDP	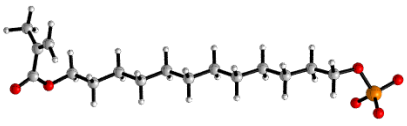		

After choosing the most preferable calcium pre-nucleation complex (8-M-4), monomers are attached in the axial position on the calcium complex. Also, we have chosen the 7-M-2 complex as a reference compound from the previous study by Mancardi *et al*.[13] to carry out an additional calculation for the interaction analysis of self-etching monomers. Several conformations of PNC-Monomer complexes are prepared by taking into account the different dihedral angles between the phosphate group of monomers and calcium ion of the PNC.

Table 5.8. 3D illustration of phosphoric acid monomers attached to PNC's 8-M-4 and 7-M-2 (M06-2X/6-31G** in water). (Color key: Ca-green, P-orange, O-red, C-grey, H-white).

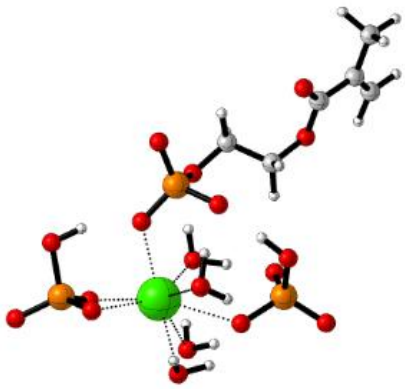

8-M-4-MEP

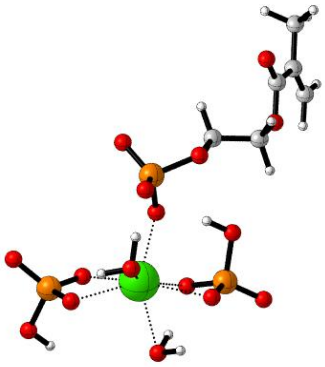

7-M-2-MEP

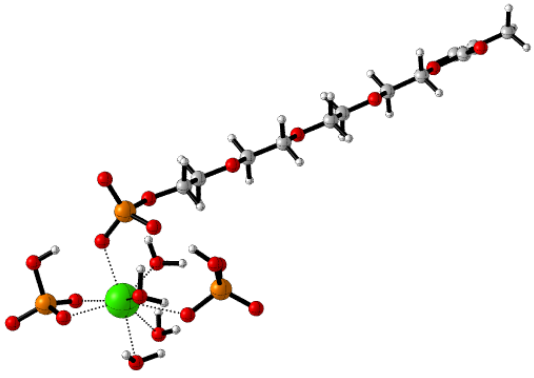

8-M-4-MTEP

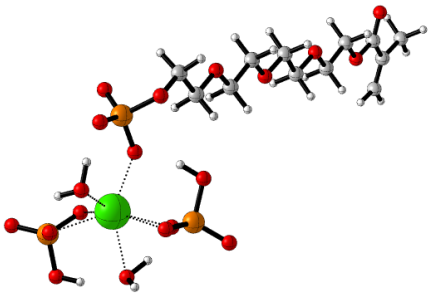

7-M-2-MTEP

Table 5.8. 3D illustration of phosphoric acid monomers attached to PNC's 8-M-4 and 7-M-2 (M06-2X/6-31G** in water). (Color key: Ca-green, P-orange, O-red, C-grey, H-white) (cont.).

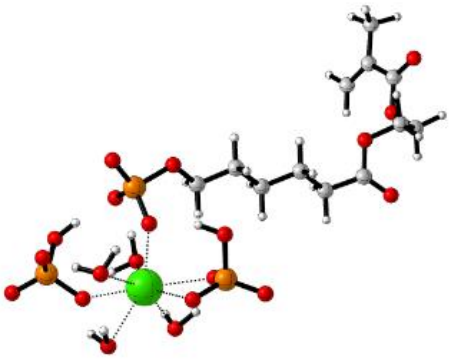

8-M-4-CAP-P

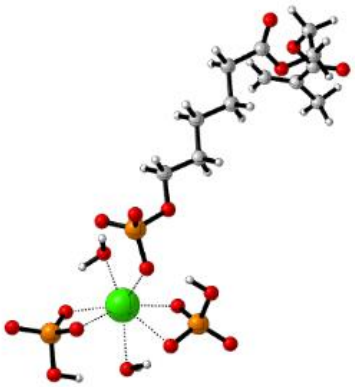

7-M-2-CAP-P

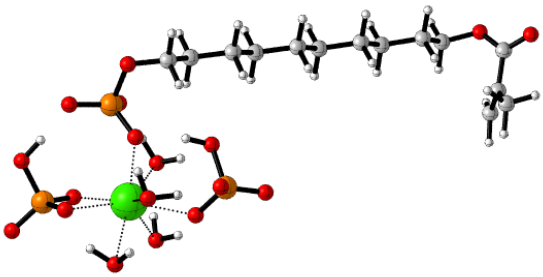

8-M-4-MDP

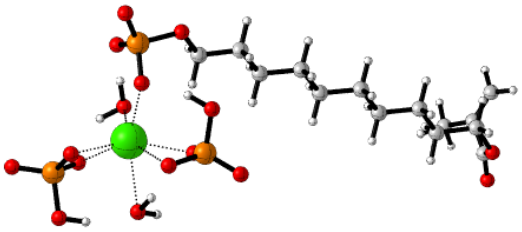

7-M-2-MDP

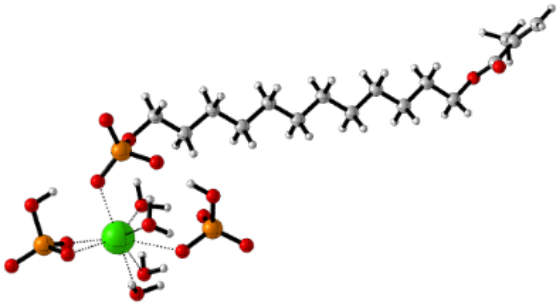

8-M-4-MDDP

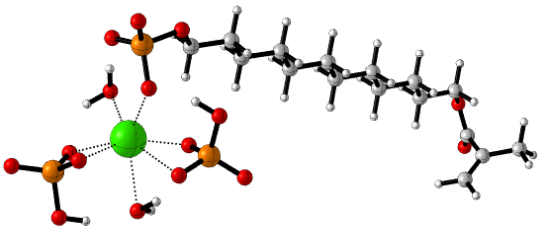

7-M-2-MDDP

Table 5.9. 3D illustration of phosphonic acid monomers attached to PNC's 8-M-4 and 7-M-2 (M06-2X/6-31G** in water). (Color key: Ca-green, P-orange, O-red, C-grey, H-white).

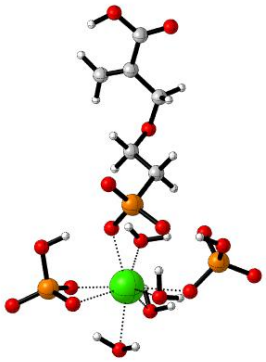

8-M-4-HAEPA

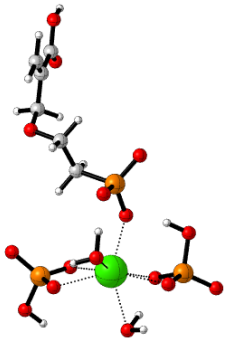

7-M-2-HAEPA

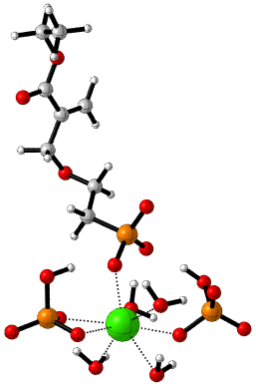

8-M-4-EAEPA

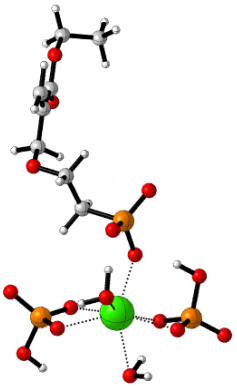

7-M-2-EAEPA

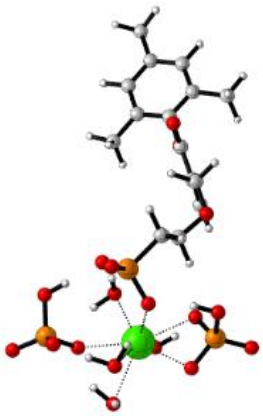

8-M-4-MAEPA

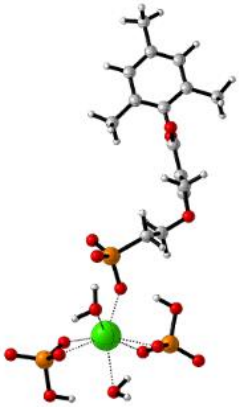

7-M-2-MAEPA

In order to compare the stabilities of the self–etching monomers onto the PNC's, and rationalize their stability order obtained by experimental studies [11, 12], the dissociation energies for the removal of monomers are calculated. The dissociation energy for the detachment of the monomers from PNC is expressed by;

$$Ca(HPO_4)_2(MON)(H_2O)_n^{-4} \rightarrow (MON)^{-2} + Ca(HPO_4)_2(H_2O)_n^{-4}$$

$$\Delta E_d = E[Ca(HPO_4)_2(H_2O)_n^{-4}] + E[(MON)^{-2}] - E[Ca(HPO_4)_2(MON)(H_2O)_n^{-4}] \quad (5.4)$$

Table 5.10. Dissociation energies (kcal/mol) for the separation of monomers from PNC 8-M-4 and 7-M-2.

COMPLEX	E_d	Rel E_d	COMPLEX	E_d	Rel E_d
8-M-4-MDDP	49.6	10.5	7-M-2-MDDP	41.7	7.4
8-M-4-MDP	46.9	7.8	7-M-2-MDP	40.5	6.2
8-M-4-CAP-P	43.7	4.6	7-M-2-CAP-P	37.8	3.5
8-M-4-MTEP	42.7	3.6	7-M-2-MTEP	36.8	2.5
8-M-4-MEP	39.9	0.8	7-M-2-MEP	35.6	1.3
8-M-4-MAEPA	46.0	6.9	7-M-2-MAEPA	39.7	5.4
8-M-4-EAEPA	43.6	4.5	7-M-2-EAEPA	36.3	2.0
8-M-4-HAEPA	39.1	0.0	7-M-2-HAEPA	34.3	0.0

According to the results obtained from Table 5.9., dissociation energies of the MDDP bonded 8-M-4 and 7-M-2 complexes were found highest with 49.6 and 41.7 kcal/mol, respectively. This indicates that the energy required to remove MDDP from PNC 8-M-4 10.5 and 9.7 kcal/mol higher than the corresponding dissociation energies of HAEPA and MEP, respectively.

The dissociation energy calculation of the monomers shed light on understanding the relation in the binding affinities of the monomers. As a result, the relation obtained from the calculations is found similar to the previous experimental studies related to the binding efficiencies of the monomers [11, 12]. In the dissociation energy calculations of both monomer attached 8-M-4 and 7-M-2 complexes, MDDP>MDP>CAP-P>MTEP>MEP and MDP>MAEPA>EAEPA>HAEPA bond strength orders were observed.

5.4.3. Analysis of the Coulombic Force

The stability of the self-etching monomers onto the surface of hydroxyapatite is due to the binding of Ca to the nearest O to oxygen as well as to the H---O interactions. In order to make a comparison between monomer stabilities, all the H---O interactions that hold the monomers on the complex are considered. The strength of the self-etching monomer and pre-nucleation complex interaction is analyzed by the calculation of coulombic forces of attractions between monomers and PNC 7-M-2. The hydrogen bonding interactions are taken into account for distances of maximum of 4 Å. The coulombic force of attractions are calculated by the equation;

$$F = \frac{|q_1 q_2|}{r^2} \qquad (5.6)$$

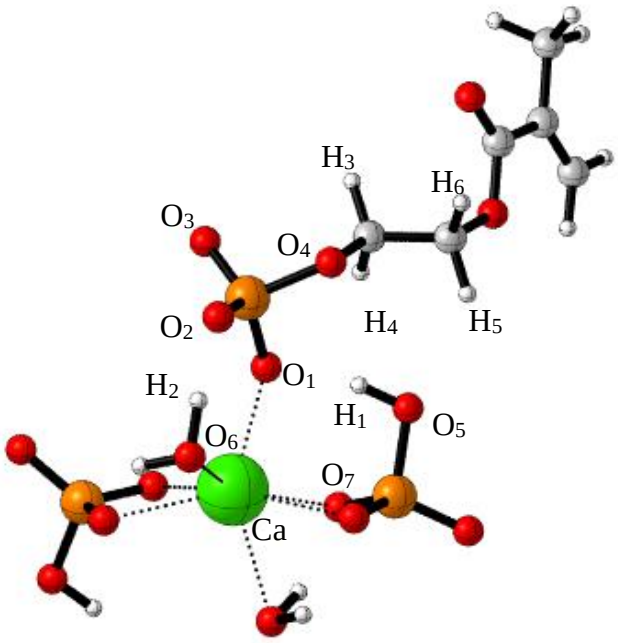

Figure.5.16. Nomenclature for 7-M-2-MEP (the same labels are used for the atoms of phosphoric acid monomers).

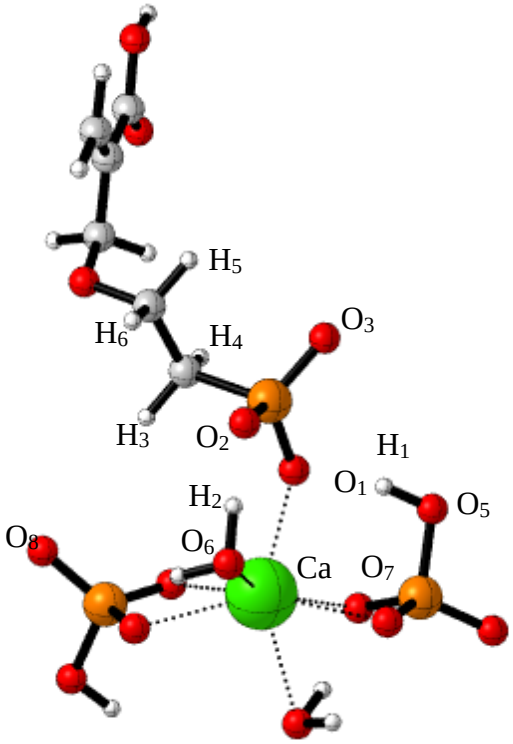

Figure 5.17. Nomenclature for 7-M-2-HAEPA (the same labels are used for the atoms of phosphonic acid monomers).

The most stable conformations of Monomer-PNC(7-M-2) complexes are indicated in tabla 5.8 and 5.9. The monomers are attached at the axial position of pre-nucleation complex, however, the phosphoric acid monomers are oriented horizontally which enables more hydrogen interaction with the pre-nucleation complex. Phosphonic acid monomers are positioned vertically, that decreases the number of hydrogen bond interaction between monomers and PNC's.

In table 5.11, it is indicated that MDDP monomer has the highest total coulombic force of attraction value which is 1.00 (au/ $Å^2$), whereas the value of MEP, the smallest phosphoric acid monomer in the group, is 0.92 (au/ $Å^2$). Additionally, the total coulombic forces of attractions are found 0.91, 0.84, 0.73 for MAEPA, EAEPA and HAEPA respectively, providing the same order obtained by binding affinity analyses of computational and experimental studies.

Table 5.11. Coulombic forces between labeled atom (au/ Å^2).

FORCE	Ca-O_1	O_1-H_1	O_2-H_2	O_4-H_1	O_5-H_5	O_6-H_3	O_7-H_4	TOTAL
7-M-2-MDDP	-0.33	-0.22	-0.28	-0.07	-0.03	-0.02	-0.05	-1.00
7-M-2-MDP	-0.33	-0.22	-0.28	-0.07	-0.04	-0.02	-0.04	-0.99
7-M-2-CAP-P	-0.32	-0.23	-0.27	-0.06	-	-0.02	-	-0.90
7-M-2-MTEP	-0.33	-0.23	-0.27	-0.06	-0.04	-	-	-0.93
7-M-2-MEP	-0.32	-0.22	-0.27	-0.07	-0.04	-	-	-0.92
	Ca-O_1	O_1-H_1	O_2-H_2	O_3-H_1	O_5-H_5	O_5-H_6	O_8-H_6	TOTAL
7-M-2-MAEPA	-0.33	-0.23	-0.29	-	-0.04	-0.03	-	-0.91
7-M-2-EAEPA	-0.32	-0.23	-0.19	-0.07	-	-	-0.03	-0.84
7-M-2-HAEPA	-0.32	-0.14	-0.19	-0.07	-	-	-0.01	-0.73

Table 5.12. Distances between labeled atoms (Å).

DISTANCE	Ca-O_1	O_1-H_1	O_2-H_2	O_4-H_1	O_5-H_5	O_6-H_3	O_7-H_4
7-M-2-MDDP	2.33	1.74	1.53	2.69	2.82	3.11	2.45
7-M-2-MDP	2.33	1.77	1.52	2.69	2.72	3.22	2.54
7-M-2-CAP-P	2.35	1.71	1.54	2.79	-	3.84	-
7-M-2-MTEP	2.32	1.72	1.55	2.76	2.47	-	-
7-M-2-MEP	2.33	1.74	1.55	2.62	2.47	-	-
	Ca-O_1	O_1-H_1	O_2-H_2	O_3-H_1	O_5-H_5	O_5-H_6	O_8-H_6
7-M-2-MAEPA	2.33	1.70	1.51	-	2.59	3.23	-
7-M-2-EAEPA	2.34	1.70	1.52	3.18	-	-	3.13
7-M-2-HAEPA	2.34	1.70	1.51	3.09	-	-	3.16

Table 5.13. NPA charges of labeled atoms (au).

CHARGE	**O_1**	**O_2**	**O_4**	**O_5**	**O_6**	**O_7**	**O_8**
7-M-2-MDDP	-1.26	-1.23	-0.91	-1.12	-1.10	-1.25	-
7-M-2-MDP	-1.26	-1.23	-0.91	-1.12	-1.10	-1.26	-
7-M-2-CAP-P	-1.25	-1.23	-0.90	-1.13	-1.10	-1.26	-
7-M-2-MTEP	-1.26	-1.23	-0.90	-1.13	-	-	-
7-M-2-MEP	-1.26	-1.23	-0.90	-1.13	-	-	-
	O_1	**O_2**	**O_3**	**O_5**	**O_6**	**O_7**	**O_8**
7-M-2-MAEPA	-1.26	-1.23	-	-1.13	-	-	-
7-M-2-EAEPA	-1.26	-1.24	-1.24	-	-	-	-1.23
7-M-2-HAEPA	-1.26	-1.24	-1.24	-	-	-	-1.23
CHARGE	**Ca**	**H_1**	**H_2**	**H_3**	**H_4**	**H_5**	**H_6**
7-M-2-MDDP	1.41	0.53	0.53	0.20	0.22	0.24	-
7-M-2-MDP	1.41	0.53	0.53	0.20	0.22	0.24	-
7-M-2-CAP-P	1.41	0.54	0.53	0.21	0.24	0.24	-
7-M-2-MTEP	1.41	0.53	0.53	-	-	0.21	-
7-M-2-MEP	1.41	0.53	0.53	-	-	0.22	-
	Ca	**H_1**	**H_2**	**H_3**	**H_4**	**H_5**	**H_6**
7-M-2-MAEPA	1.41	0.53	0.53	-	-	0.23	0.25
7-M-2-EAEPA	1.41	0.53	0.53	-	-		0.25
7-M-2-HAEPA	1.41	0.53	0.53	-	-		0.24

The results obtained from the calculation of total coulombic force of attraction for the atoms within 4Å distance show that the monomers having longer spacer (R) group has a greater total coulombic force of attraction values due to their closer orientation through the pre-nucleation complex (Table 5.11). The higher value of the total force is expected to provide better stability and higher dissociation energy of monomers. The stability of monomers is found proportional to the amount of total coulombic forces of attraction in between monomers and pre-nucleation complex.

6. CONCLUSION

This dissertation has carried out a computational investigation on i) the cyclopolymerization reaction of bistyrenic monomers and ii) the binding affinities of self-etching monomers on the surface of the tooth. For the former, the efficiency of tethering groups in cyclopolymerization reactions was discussed. For the latter, several commonly used self-etching monomers are evaluated, and their binding affinities towards the tooth surface were compared.

The efficient cyclopolymerization of bistyrenic monomers with silyl-based and malonate ester tether groups has been previously indicated in the experimental study by. Dario Pasini *et.al.* [8]. Along with the cyclopolymerization reaction, the control over the sequence of styrene monomer is provided. In this reaction, two styrenic monomers are connected to each other by a tether group which is able to orient two monomeric units. In order to provide improvements in the linkage system of styrenic moieties, silyl-based tethers are proposed after malonate ester tethers. The advantages of the silyl-based tethers are their commercial availability and the easiness of their removal from the polymeric chain during deprotonation step after cyclopolymerization reaction is completed. In this thesis, the calculations for the cyclopolymerization reaction of bistyrenic monomers with the tethering groups are performed by DFT at M06-2X/6-31G* level. By rationalization of the experimental findings with computational tools, it is indicated that the computational approach can be used to evaluate the tethering groups in the initial stages of free radical cyclopolymerization reaction. The results have shown that silyl-based monomers can be used efficiently as an alternative to the previously proposed malonate ester tethering group.

Modeling the initiation, cyclization, and propagation of M1, M2, M3 has revealed the fact that these three reactions proceed in the same way without a considerable difference in the Gibbs Free energies for similar steps. This similar trend in the reaction profile shows that sily-based monomers undergo cyclopolymerization reaction as good as malonate ester groups. In all three steps of the reaction, the rate determining steps are found the initiation and propagation steps. Cyclization is more facile than the others due to its lower activation barrier. Both initiation, cyclization and propagation steps found quite exergonic. The Gibbs

Free Energy of activation for M2 (diphenyl-silyl tether) is lower in each step, hence M2 is slightly more favorable than the corresponding steps of M1 (malonate ester tether) and M3 (methyl(phenyl)-silyl tether).

In the second chapter, the ground state properties of self-etching phosphoric and phosphonic acid monomers are investigated computationally. In order to compare the binding affinities of self-etching monomers onto the surface of the tooth, pre-nucleation complexes are taken into account as a representative structure for the hydroxyapatite component of the tooth. The general structure of the pre-nucleation complex has been indicated in the experimental studies of Habreken *et al.* [34], in which three phosphates are bonded to calcium ion to form the complex having -4 charge. However, due to the absence of a general agreement with the most stable structure of pre-nucleation complex which forms hydroxyapatite through precipitation, in this work, its several conformations are illustrated and they are optimized by using DFT. As a result of the calculations at M06-2X/6-31G** (in water), 8 coordinated calcium triphosphate complex with 4 water molecules is found the most stable pre-nucleation complex having the minimum energy among its other corresponding alternatives. Regarding the most stable complex (8-M-4), one of the important observations is that, although calcium ion is expected to form 6 coordinated calcium-water complex [43] the PNC tends to have 8 coordination number when three phosphate groups and water molecules are bound to calcium. Therefore, among the different conformations of the PNC's which have the same amount of water and phosphates, varying only by the coordination number, the complexes with 8 coordination number are energetically more favorable than their other conformations. Additionally, monodentate binding type of the phosphates in the axial position has the ability to decrease the energy of the complex. The monodentate binding type of the axial phosphates causes its Ca-O bond distance to be smaller compared to Ca-O bond distances of bidentate axial phosphates. It is also emphasized that the complex is stabilized by the hydrogen interaction with water molecules and other phosphate groups within the complex. The complexes having more intramolecular hydrogen bondings are found energetically more stable.

Since the most stable PNC in the study is found to be 8-M-4, self-etching monomers are attached at the axial position of the complex. After the conformational analysis of the monomer-PNC structures, the dissociation energy of the self-etching monomers are

calculated in order to analyze the binding strength of the monomers to the calcium ion in pre-nucleation complex 8-M-4. The same procedure is followed for the illustration of self-etching monomer and PNC 7-M-2 interaction. The dissociation energy calculations which shows the energy required to remove the monomers from the PNC are indicated and the stability order between monomers is found identical to the order proposed by the previous experimental studies [11, 12]. The stability order obtained from the dissociation energy calculations is MDDP>MDP>CAP-P>MTEP>MEP and MAEPA>EAEPA>HAEPA. The energy cost to remove MDDP from the PNC 8-M-4 is approximately 10.5 and 9.7 kcal/mol higher than HAEPA and MEP, respectively. When the same calculations are carried out for the monomers with PNC 7-M-2, the dissociation energy of MDDP is found 7.4 and 6.1 and kcal/mol higher than HAEPA and MEP, respectively.

In this thesis, the computational approach indicates approximate results to the experimental analysis of self-etching monomers. Hence, the computational method enables the interaction between self-etching monomer and pre-nucleation complex to be understood at an atomic level and it can be used for the further evaluation of self-etching monomers in large scales. The biggest advantage of the method is the fact that it enables the analysis of a wide range of self-etching monomers, especially the ones that are newly-designed. The fast evaluation of monomers with this method allows time-saving during the experimental search for the broad amount of monomers. In that way, the cost of the experimental work concerning the improvements of self-etching monomers can be diminished and the possibilities to find more efficient monomers can be filtered using the computational approach.

REFERENCES

1. L. H. Sperling, *Introduction to Physical Polymer Science*, vol. 207, no. 8. 2006.

2. R. O. Ebewele, "Polymer Properties and Applications," in *Polymer Science and Technology*, 2000.

3. G. Odian, *Principles of Polimerization*, vol. 58, no. 6. 2004.

4. C. L. Huang, Y. C. Chen, T. J. Hsiao, J. C. Tsai, and C. Wang, "Effect of tacticity on viscoelastic properties of polystyrene," *Macromolecules*, vol. 44, no. 15, pp. 6155–6161, 2011.

5. J. F. Lutz, M. Ouchi, D. R. Liu, and M. Sawamoto, "Sequence-controlled polymers," *Science*, vol. 341, no. 6146. 2013.

6. T. Kakuchi and M. Obata, "Synthesis and mechanism of a main-chain chiral polymer based on asymmetric cyclopolymerization," *Macromolecular Rapid Communications*, vol. 23, no. 7. pp. 395–406, 2002.

7. G. B. Butler, "Cyclopolymerization," *J. Polym. Sci. Part A Polym. Chem.*, vol. 38, no. 19, pp. 3451–3461, 2000.

8. N. Ferri, G. B. Ozaydin, A. Zeffiro, A. Nitti, V. Aviyente, and D. Pasini, "The efficient cyclopolymerization of silyl-tethered styrenic difunctional monomers," *J. Polym. Sci. Part A Polym. Chem.*, vol. 56, no. 14, pp. 1593–1599, 2018.

9. M. Mathew and S. Takagi, "Structures of Biological Minerals in Dental Research," *J. Res. Natl. Inst. Stand. Technol.*, vol. 106, no. 6, pp. 1035–1044, 2001.

10. N. Moszner and U. Salz, "Chemical aspects of self-etching enamel – dentin adhesives : A systematic review," *Dent. Mater.*, vol. 21, no. 10, pp. 895–910, 2005.

11. K. Yoshihara and A. O. Ogliari, “Can the Hydrophilicity of Functional Monomers Affect Chemical Interaction ?,” *J. Dent. Res.*, vol. 93, no. 2, pp. 201–206, 2014.

12. K. L. Van Landuyt, Y. Yoshida, and H. *et al*. Al., “Influence of the Chemical Structure of Functional Monomer,” *J. Dent. Res.*, vol. 87, no. 8, pp. 757–761, 2008.

13. G. Mancardi, U. Terranova, and N. H. De Leeuw, “Calcium Phosphate Prenucleation Complexes in Water by Means of ab Initio Molecular Dynamics Simulations,” *Cryst. Growth Des.*, vol. 16, no. 6, pp. 3353–3358, 2016.

14. S. Edizer, B. Veronesi, O. Karahan, V. Aviyente, I. Değirmenci, A. Galbiati, and D. Pasini, “Efficient Free-Radical Cyclopolymerization of Oriented Styrenic Difunctional Monomers,” *Macromolecules*, vol. 42, no. 6, pp. 1860–1866, Mar. 2009.

15. T. K. Vaidyanathan and J. Vaidyanathan, “Review Recent Advances in the Theory and Mechanism of Adhesive Resin Bonding to Dentin : A Critical Review,” pp. 558–578, 2008.

16. A. R. Leach, “Molecular modelling : principles and applications Second Edition,” *Pearson Educ. EMA*, p. 784, 2001.

17. C. J. Cramer, *Essentials of Computational Chemistry: Theories and Models*. 2004.

18. R. Peverati and D. G. Truhlar, “Quest for a universal density functional: The accuracy of density functionals across a broad spectrum of databases in chemistry and physics,” *Philosophical Transactions of the Royal Society A: Mathematical, Physical and Engineering Sciences*, vol. 372, no. 2011. 2014.

19. S. F. Sousa, P. A. Fernandes, and M. J. Ramos, “General performance of density functionals,” *J. Phys. Chem. A*, vol. 111, no. 42, pp. 10439–10452, 2007.

20. N. Engineering, “Evaluation of B3LYP , X3LYP , and M06-Class Density Functionals for Predicting the Binding Energies of Neutral , Protonated , and

Deprotonated Water Clusters," *J. Chem. Theory Comput.*, pp. 1–14, 2008.

21. Y. Zhao, D. G. Truhlar, Y. Zhao, and D. G. Truhlar, "The M06 suite of density functionals for main group thermochemistry, thermochemical kinetics, noncovalent interactions, excited states, and transition elements: two new functionals and systematic testing of four M06-class functionals and 12 other functionals," *Theor Chem Acc.*, vol. 120, pp. 215–241, 2008.

22. T. Helgaker, P. Jørgensen, and J. Olsen, "Gaussian Basis Sets," in *Molecular Electronic-Structure Theory*, 2000.

23. J. Tomasi, B. Mennucci, and R. Cammi, "Quantum mechanical continuum solvation models," *Chemical Reviews*, vol. 105, no. 8. pp. 2999–3093, 2005.

24. C. J. Cramer and D. G. Truhlar, "Implicit Solvation Models: Equilibria, Structure, Spectra, and Dynamics," *Chem. Rev.*, vol. 99, no. 8, pp. 2161–2200, 1999.

25. B. Vincenzo, C. Maurizio, and T. Jacopo, "Geometry optimization of molecular structures in solution by the polarizable continuum model," *J. Comput. Chem.*, vol. 19, no. 4, pp. 404–417, 1998.

26. V. Barone and M. Cossi, "Quantum calculation of molecular energies and energy gradients in solution by a conductor solvent model," *J. Phys. Chem. A*, vol. 102, no. 11, pp. 1995–2001, 1998.

27. B. Mennucci, E. Cancès, and J. Tomasi, "Evaluation of Solvent Effects in Isotropic and Anisotropic Dielectrics and in Ionic Solutions with a Unified Integral Equation Method: Theoretical Bases, Computational Implementation, and Numerical Applications," *J. Phys. Chem. B*, vol. 101, no. 49, pp. 10506–10517, 1997.

28. B. Mennucci and J. Tomasi, "Continuum solvation models: A new approach to the problem of solute's charge distribution and cavity boundaries," *J. Chem. Phys.*, vol. 106, no. 12, pp. 5151–5158, 1997.

29. R. Grubbs, C. Bielawski, and D. Benitez, “An’Endless’ Route to Cyclic Polymers,” *Science (80-.).*, vol. 297, no. 5589, pp. 2041–2045, 2002.

30. M. J. Frisch, G. W. Trucks, H. B. Schlegel, and E. Al., “Gaussian09.,” *Gaussian 09*. 2009.

31. Y. R. Zhang, W. Du, X. D. Zhou, and H. Y. Yu, “Review of research on the mechanical properties of the human tooth,” *International Journal of Oral Science*, vol. 6, no. 2. pp. 61–69, 2014.

32. J. I. Rosales, G. W. Marshall, S. J. Marshall, L. G. Watanabe, M. Toledano, M. A. Cabrerizo, and R. Osorio, “Acid-etching and hydration influence on dentin roughness and wettability,” *J. Dent. Res.*, vol. 78, no. 9, pp. 1554–1559, 1999.

33. Larry Li, “Structure of the Tooth,” 2014. [Online]. Available: https://biologydictionary.net/teeth/.

34. W. J. E. M. Habraken, J. Tao, L. J. Brylka, H. Friedrich, L. Bertinetti, A. S. Schenk, A. Verch, V. Dmitrovic, P. H. H. Bomans, P. M. Frederik, J. Laven, P. Van Der Schoot, B. Aichmayer, G. De With, J. J. DeYoreo, and N. A. J. M. Sommerdijk, “Ion-association complexes unite classical and non-classical theories for the biomimetic nucleation of calcium phosphate,” *Nat. Commun.*, vol. 4, pp. 1507–1512, 2013.

35. F. Betts and A. S. Posner, “An X-ray radial distribution study of amorphous calcium phosphate,” *Mater. Res. Bull.*, vol. 9, no. 3, pp. 353–360, 1974.

36. P. *et al*. Besenius, “Controlling the growth and shape of chiral supramolecular polymers in water.,” *Proc. Natl Acad. Sci. USA*, vol. 107, pp. 17888–17893, 2010.

37. N. Almora-Barrios and N. H. De Leeuw, “Molecular dynamics simulation of the early stages of nucleation of hydroxyapatite at a collagen template,” *Cryst. Growth Des.*, vol. 12, no. 2, pp. 756–763, 2012.

38. E. Bruzzi and A. J. Stace, “Experimental measurements of water molecule binding energies for the second and third solvation shells of [Ca(H2O)n]2+complexes,” *R. Soc. Open Sci.*, vol. 4, no. 1, 2017.

39. X. L. Lei and B. C. Pan, “Structures, stability, vibration entropy and IR spectra of hydrated calcium ion clusters [Ca(H2O)n]2+ (n = 1-20, 27): A systematic investigation by density functional theory,” *J. Phys. Chem. A*, vol. 114, no. 28, pp. 7595–7603, 2010.

40. J. M. C. Marques, F. B. Pereira, P. E. Abreu, M. Albertí, A. Aguilar, F. Pirani, and M. Bartolomei, “A global optimization perspective on molecular clusters Subject Areas :,” 2017.

41. M. Peschke, A. T. Blades, and P. Kebarle, “Hydration Energies and Entropies for Mg^{2+}, Ca^{2+}, Sr^{2+}, and Ba^{2+} from Gas-Phase Ion−Water Molecule Equilibria Determinations,” *J. Phys. Chem. A*, vol. 102, no. 48, pp. 9978–9985, 1998.

42. M. F. Bush, R. J. Saykally, and E. R. Williams, “Hydration of the calcium dication: Direct evidence for second shell formation from infrared spectroscopy,” *ChemPhysChem*, vol. 8, no. 15, pp. 2245–2253, 2007.

43. D. R. Carl, R. M. Moision, and P. B. Armentrout, “Binding energies for the inner hydration shells of Ca2+: An experimental and theoretical investigation of Ca2+(H2O)xcomplexes (x = 5-9),” *Int. J. Mass Spectrom.*, vol. 265, no. 2–3, pp. 308–325, 2007.

44. V. I. Chizhik, A. V Egorov, M. S. Pavlova, M. I. Egorova, and A. V Donets, “Structure of hydration shell of calcium cation by NMR relaxation , Car-Parrinello molecular dynamics and quantum-chemical calculations,” *J. Mol. Liq.*, vol. 224, pp. 730–736, 2016.